Evaluation of Mei-yu Heavy-Rainfall Quantitative Precipitation Forecasts in Taiwan by A Cloud-Resolving Model for Three Seasons of 2012-2014

Chung-Chieh Wang[1], Pi-Yu Chuang[1]*, Chih-Sheng Chang[1], Kazuhisa Tsuboki[2], Shin-Yi Huang[1], and Guo-Chen Leu[3]

1 Department of Earth Sciences, National Taiwan Normal University, Taipei, Taiwan
2 Institute for Space-Earth Environmental Research, Nagoya University, Nagoya, Japan
3 Central Weather Bureau, Taipei, Taiwan

Corresponding author: Pi-Yu Chuang (giselle780507@hotmail.com)

Abstract.

In this study, the performance of quantitative precipitation forecasts (QPFs) by the Cloud-Resolving Storm Simulator (CReSS) in Taiwan, at a horizontal grid spacing of 2.5 km and a domain size of 1500×1200 km^2, at the ranges of 1-3 days during three mei-yu seasons (May-June) of 2012-2014 is evaluated using categorical statistics, with an emphasis on heavy rainfall events (≥ 100 mm per 24 h). The categorical statistics are chosen because the main hazards are landslides and floods in Taiwan, so predicting heavy rainfall at the correct location is important. The overall threat scores (TSs) of QPFs for all events on day 1 (0-24 h) are 0.18, 0.15, and 0.09 at the threshold of 100, 250, and 500 mm, respectively, and indicate considerable improvements at increased resolution compared to past results and 5-km models (TS < 0.1 at 100 mm and TS ~ 0 at 250 mm).

Moreover, the TSs are shown to be higher and the model more skillful in predicting larger events, in agreement with earlier findings for typhoons. After classification based on observed rainfall, the TSs of day-1 QPFs for the largest 4% of events by CReSS at 100, 250, and 500 mm (per 24 h) are 0.34, 0.24, and 0.16, respectively, and can reach 0.15 at 250 mm on day 2 (24-48 h) and 130 mm on day 3 (48-72 h). The larger events also exhibit higher probability of detection and lower false alarm ratio than smaller ones almost without exception across all thresholds. With the convection and terrain better resolved, the strength of the model is found to lie mainly in the topographic rainfall in Taiwan rather than migratory events that are more difficult to predict. Our results highlight the crucial importance of cloud-resolving capability and the size of fine mesh for heavy-rainfall QPFs in Taiwan.

1 Introduction

The Quantitative Precipitation Forecasting (QPF) is one of the most challenging areas in modern numerical weather prediction (e.g., Golding, 2000; Fritsch and Carbone, 2004; Cuo et al., 2011), especially for extreme events that have high potential for hazards. With its steep and complex topography, Taiwan over the western North Pacific (Fig. 1) experiences extreme rainfall rather frequently, mainly during two periods: the typhoon (July-October) and mei-yu (May-June) seasons (e.g., Kuo and Chen, 1990; Wu and Kuo, 1999; Jou et al., 2011; Chang et al., 2013). The landslides and flash floods in/near the mountains and flooding over low-lying plains and urban areas are the main hazards (e.g., Wang et al., 2012b, 2013b, 2016b). In order to better prepare for these hazards and reduce their impacts, QPFs and their verifications, especially over heavy-rainfall thresholds from large events, are thus very important for Taiwan. Of course, to identify where the model can make significant improvements in QPFs and what approaches are effective to achieve them are also crucial (e.g., Clark et al., 2011).
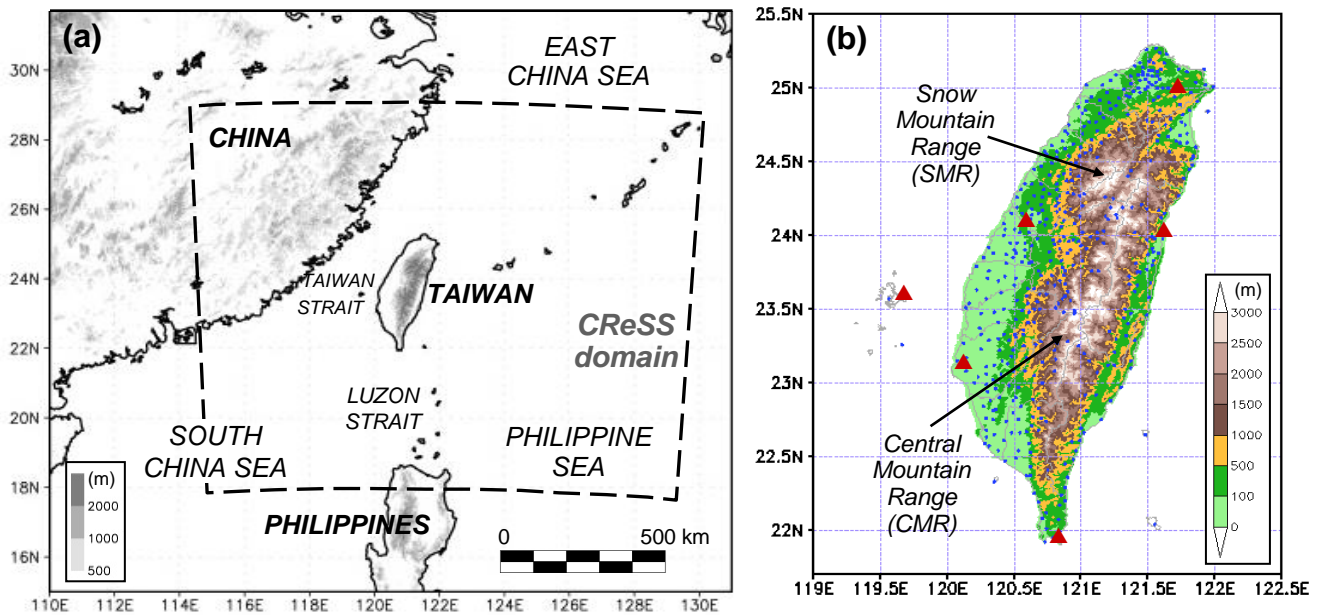
Figure 1: (a) The geography and topography (m, shading) surrounding Taiwan and the domain of 2.5-km CReSS (thick dashed box), and (b) the detailed terrain of Taiwan (m, color) and the locations of rain gauges (blue dots) and land-based radars (scarlet triangles) used to produce the reflectivity composites by the Central Weather Bureau (CWB). The two major mountain ranges in Taiwan, the Central Mountain Range (CMR) and Snow Mountain Range (SMR), are marked in (b).

For the mei-yu season in Taiwan, earlier studies mainly employed the widely-used, standard categorical measures (see Section 2.4) to evaluate the performance of models such as the Mesoscale Model version 5 (MM5) at thresholds up to 50 mm per 12 h (e.g., Chien et al., 2002, 2006; Yang et al., 2004). Their results show that the models at the time had some ability in predicting rainfall occurrence at thresholds ≤ 2.5 mm, but little skill at 50 mm and above. In recent years, several studies (e.g., Hsu et al., 2014; Li and Hong, 2014; Su et al., 2016; Huang et al., 2016) have also examined the QPFs by the Weather Research and Forecasting (WRF) model (Skamarock et al., 2005) running at the Central Weather Bureau (CWB) at 5-km grid spacing (Δx), including its ensembles. These studies indicate improvements over earlier models at thresholds up to 50-100 mm (per 12 h) over the previous decade. However, the accuarcy at 150-200

54 mm and beyond is still limited, even with probability-matching (e.g., Ebert, 2001) within the forecast range of 24 h

55 (see e.g., Figs. 9 and 10 of Huang et al., 2016).

56 Figure 2 shows the threat scores (TSs) of day-1 (0-24 h) and day-2 (24-48 h) QPFs for May and June of 2013 and

57 2014 by the CWB models as an example. The TS is defined as the fraction of hits among all verification points that

58 are either observed or predicted, or both, at the specified rainfall threshold, and thus $0 \leq TS \leq 1$ (further details in

59 Section 2.4). The CWB models include deterministic WRF and several products from their 20-member WRF ensemble

60 prediction system (WEPS, e.g., Hong et al., 2015), all with $\Delta x = 5$ km. These plots are produced for each month at the

61 CWB for routine verification (within a range of 48 h) since 2013, and are similar to those in Huang et al. (2015, 2016).

62 In addition to deterministic forecasts, the scores also include those using probability-matching techniques (PM and

63 NPM, e.g., Ebert, 2001; Fang and Kuo, 2013), which may provide some benefit over the ensemble mean (WEPS) for

64 thresholds between 50-200 mm (e.g., Su et al., 2016; Huang et al., 2016). In Fig. 2, one can see that the TSs are no

65 higher than 0.07 at 100 mm (per 24 h) and 0.03 at 200 mm (and TS = 0 at and above 300 mm) for either day 1 or day

66 2 in the two mei-yu seasons, in line with the review above. The scores in June also tend to be lower compared to May,

67 likely due to more events of thermally-driven, localized rainfall with low predictability (e.g., Chen and Chen, 2003;

68 Chen et al., 1999; Paul et al., 2018). Nevertheless, effective strategies and methods to improve the skill level at

69 thresholds near 100-150 mm and beyond are needed.

70 Wang (2015, hereafter referred to as W15) evaluated the QPFs, within 3 days, by a cloud-resolving model (CRM),

71 the Cloud-Resolving Storm Simulator (CReSS; Tsuboki and Sakakibara, 2002, 2007), for all 15 typhoons that hit

72 Taiwan in 2010-2012. With $\Delta x = 2.5$ km, a grid size more comparable to research studies (e.g., Wang et al., 2005,

73 2011; 2013a, also Bryan et al., 2003; Done et al., 2004; Clark et al., 2007; Roberts and Lean, 2007), these deterministic

74 forecasts showed superior performance in QPFs, with TSs of 0.38, 0.32, and 0.16 at thresholds of 100, 250, and 500

75 mm, respectively, for all typhoons on day 1 (0-24 h, cf. his Fig. 13). Even on day 3 (48-72 h), the corresponding TSs

76 are 0.21, 0.12, and 0.01. Thus, the accuracy of QPFs by this CRM over the thresholds of 100-500 mm is remarkably

77 higher for typhoon rainfall in Taiwan.

78 Moreover, as summarized in Wang (2016), W15 found a strong positive dependency of categorical scores on overall

79 rainfall amount (which represents event magnitude). That is, the larger the rain, the higher the scores, and the better

80 the model performs. For example, the TSs at the same thresholds (100, 250, and 500 mm) for his top-5 events (roughly

81 top 5%) on day 1 are 0.68, 0.49, and 0.24, respectively (Fig. 1 of Wang, 2016), all at least 1.5 times higher than their

82 counterparts for all typhoons. An important implication of this finding is that the model QPFs for extreme events *may*

83 *not* be accurately assessed through categorical statistics without proper classification to isolate them from ordinary

84 events, and particularly not by taking arithmetic mean of TSs of multiple forecasts. The study of W15 also predicts

85 the dependency, as a fundamental property, to exist in other rainfall regimes. Therefore, the main purpose of this study

86 is three-fold: 1) to assess the ability of the 2.5-km CReSS in predicting mei-yu rainfall at a higher resolution than

87 before, especially for heavy to extreme rainfall events, 2) to clarify whether the dependency property in categorical

88 scores also exists in the mei-yu regime in Taiwan? and 3) if the QPFs by CReSS prove to be improved, why or where

89 its strength lies?

90

91
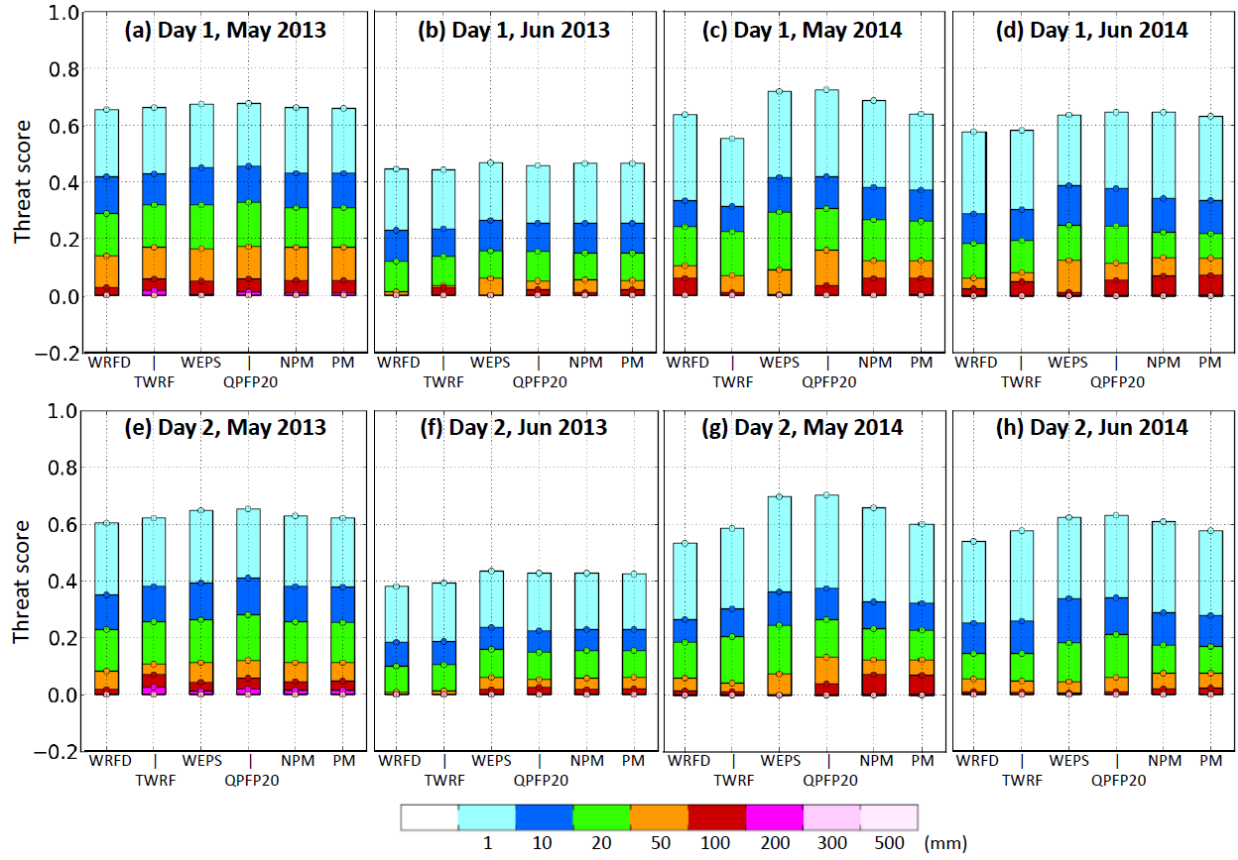
Figure 2: The TS of 0-24-h QPFs (day 1) for (a) May and (b) Jun of 2013, and (c) May and (d) Jun of 2014, respectively, at selected thresholds over 1-500 mm (per 24 h, scale at bottom) by two deterministic forecasts from WRF (WRFD) and the Typhoon WRF (TWRF) and four ensemble forecasts from the 20-member WRF Ensemble Prediction System: ensemble mean (WEPS), top 20% (QPFP20), and WEPS employing the probability matching (PM) and new PM (NPM) techniques. (e)-(h) As in (a)-(d), but showing the TS of 24-48-h QPFs (day 2), respectively.

In Section 2, the model, data, and methodology are described. In Section 3, the overall scores of QPFs for groups with different event magnitudes are presented and compared with previous results. Then in Section 4, examples are selected to illustrate how the CRM performs in real-time forecasts and where its strength lies. Aspects related to the dependency property are further discussed in Section 5, and our conclusions are given in Section 6.

2 Data and Methodology

2.1 The CReSS model and its forecasts

The CReSS model is a non-hydrostatic, compressible CRM with a single domain without intermediate nesting (Tsuboki and Sakakibara, 2002, 2007), and it has been used for weather forecasts in Taiwan since 2006 (http://cressfcst.es.ntnu.edu.tw/, W15; Wang et al., 2013, 2016a). Starting from July 2010, a grid size of 2.5 km is utilized, with a domain of 1500×1200 km^2 since May 2012 (Fig. 1a and Table 1). In CReSS, cloud formation, development, and all related processes are explicitly treated using a bulk cold-rain microphysical scheme with six species (Lin et al., 1983; Cotton et al., 1986; Murakami, 1990; Ikawa and Saito, 1991; Murakami et al., 1994): vapor, cloud water, cloud ice, rain, snow, and graupel (Table 1). Thus, no cumulus (or shallow convection) parameterization

110   is used. Other sub-grid scale processes parameterized in the model include turbulent mixing in the planetary boundary
111   layer with a 1.5-order closure (Deardorff, 1980; Tsuboki and Sakakibara, 2007), as well as surface radiation and
112   momentum/energy fluxes (Kondo, 1976; Louis et al., 1982; Segami et al., 1989). These physical options are identical
113   to W15, and also given in Table 1.

Season	2012	2013 and 2014
Projection	Lambert Conformal (center at 120°E, secant at 10°N and 40°N)	
Grid spacing (km)	$2.5 \times 2.5 \times 0.2\text{-}0.663 \ (0.5)^{*}$	
Grid dimension (x, y, z)	$600 \times 480 \times 40$	
Domain size (km)	$1500 \times 1200 \times 20$	
Forecast frequency	Every 6 h (at 0000, 0600, 1200, and 1800 UTC)	
Forecast range	72 h	78 h
IC/BCs (including sea surface temperature)	NCEP GFS analyses/forecasts (at 26 levels)	
	$1° \times 1°$	$0.5° \times 0.5°$
Topography	Real at $(1/120)°$ spatial resolution (~0.9 km)	
Cloud microphysics	Bulk cold-rain scheme (Lin et al., 1983; Cotton et al., 1986; Murakami, 1990; Ikawa and Saito, 1991; Murakami et al., 1994)	
PBL/turbulence	1.5-order closure with prediction of turbulent kinetic energy (Deardorff, 1980; Tsuboki and Sakakibara, 2007)	
Surface processes	Energy/momentum fluxes, shortwave and longwave radiation (Kondo, 1976; Louis et al., 1982; Segami et al., 1989)	
Substrate model	41 levels, every 5 cm to 2 m	

114   **Table 1: The basic configuration, initial/boundary conditions (IC/BCs), and physical packages of the 2.5-km CReSS used**
115   **for real-time operation in 2012-2014. * The vertical grid spacing of CReSS is stretched (smallest at bottom), and the averaged**
116   **spacing is given in the parentheses.**

117   The operational analyses and forecasts by the Global Forecasting System (GFS, Kanamitsu, 1989; Kalnay et al., 1990;
118   Moorthi et al., 2001; Kleist et al., 2009) of the National Centers for Environmental Prediction (NCEP), produced every
119   6 h (at 26 levels), were used as initial and boundary conditions (IC/BCs) for CReSS (Table 1). The CReSS model is
120   also run four times a day, each out to 72 h (now 78 h). At the lower boundary, terrain data at 30" resolution (roughly
121   900 m) and the NCEP analyzed sea surface temperature are also provided. With its limited domain size, the
122   atmospheric evolution in CReSS is forced by the NCEP forecasts, especially at longer ranges. Note that since 2013,
123   the IC/BCs from the GFS have increased the resolution from $1° \times 1°$ to $0.5° \times 0.5°$, but all other settings are kept the
124   same during our study period (Table 1).

125   **2.2 Data**

126   The observational data used include synoptic weather maps from the CWB, the vertical maximum indicator reflectivity
127   composites every 30 min from land-based radars, and hourly rainfall data from about 440 gauges in Taiwan for QPF
128   verification (Fig. 1b). Along with NCEP gridded final analyses (on $1° \times 1°$ grid), the weather maps are used to identify

129 and synthesize the occurrence of favorable factors to heavy rainfall among events with different magnitude (to be
130 described in Section 2.3). For selected heavy-rainfall cases, the radar composites are compared with the CReSS
131 forecasts to assess the quality of the QPFs in Section 4.

Group	Criterion (of 10% gauges)	No. of segments (%)	No. of all points (N)	No. of points (H + M + FA) at threshold (mm)			
				50	100	250	500
A+	≥ 130 mm (a subset of A)	13 (3.9)	5622	3807	2453	490	32
A	≥ 50 mm	61 (18.1)	26826	11000	4889	675	47
B	≥ 25 mm, but not A	75 (22.3)	33018	4279	1078	98	4
C	≥ 10 mm, but not B	88 (26.1)	38583	1675	281	10	3
D	≥ 1 mm, but not C	67 (19.9)	29267	266	32	0	0
X	< 1 mm	46 (13.6)	20067	59	20	4	0
All	A through D plus X	337 (100.0)	147761	17279	6300	787	54

132 **Table 2: The classification criteria using (at least) 10% of rain gauges with highest 24-h accumulated rainfall (0000-2400 or**
133 **1200-1200 UTC) over Taiwan, and the results in the number of 24-h segments (and percentage) and total points (sites) of H**
134 **+ M + FA at selected rainfall thresholds (mm) for the different groups. During the mei-yu seasons of 2012-2014, the total N**
135 **is 148776 and on average there are 442 rain gauges per segment. The points of H + M + FA are based on the statistics of**
136 **day-1 (0-24 h) QPFs, and N is also given (with no threshold).**

137 **2.3 Verification period classification**

138 In this study, objective categorical statistics (e.g., Schaefer, 1990; Wilks, 2011) are used to verify QPFs mainly because:
139 1) the ability of models to predict the heavy rainfall at the correct location is imperative in Taiwan, since its primary
140 hazards are landslides and floods, and 2) our results can be easily compared with earlier studies. Here, 24-h QPFs are
141 chosen because: 1) the bulk rainfall accumulation from mei-yu events, as for typhoons, is our main concern rather
142 than the rain over shorter periods, especially at longer ranges (days 2-3), and 2) the issue of double penalty on high-
143 resolution QPFs (e.g., Ebert and McBride, 2000) is less serious using a longer accumulation period. Although the
144 CReSS forecasts are made four times a day, only those from 0000 and 1200 UTC are evaluated in this study.
145 A total of 366 target segments (0000-2400 and 1200-1200 UTC) in May-June, 2012-2014 are classified into several
146 groups based on the observed rainfall using the following criteria, as summarized in Table 2. Groups A, B, C, and D
147 are those periods with at least 10% rain gauges reaching 50, 25-50, 10-25, and 1-10 mm, respectively, while group X
148 is the remaining periods with little or no rain. The full classification results (Table 3) give a total of 337 segments,
149 excluding those under typhoon influence. Groups A-D individually account for about 18-26% and are comparable in
150 sample size, while the driest group X is about 14% (Tables 2 and 3). These five groups are exclusive to each other,
151 and the results without classification will be referred to as the "all" group. From group A, a subset of A+ that has ≥
152 10% sites reaching 130 mm is identified and represents the most-rainy 4% in our sample with the highest hazard
153 potential. The spatial distribution of mean mei-yu rainfall per season in 2012-2014, with a peak amount of about 1700
154 mm, is shown in Fig. 3 and resembles the climatology (e.g., Yeh and Chen, 1998; Chien and Jou, 2004; Chi, 2006;
155 Wang et al., 2017).

Year	Month	Time (UTC)	Date in month			Segments included (A-D, X)
			1-10	11-20	21-31 (or 21-30)	
2012	May	0000	XAABDXXXBB	CCXXCBAAAB	XXDXDCAAABC	31
		1200	CAADXXXBCC	CXXCBBAB**A**D	XXXXDBAABBD	31
	Jun	0000	CCBCCCCB**AA**	**AAA**AABBTTT	TCCDDCTTTD	23
		1200	DBCDCDBA**AA**	**A**AAABBTTTT	TCDDDTTTTD	21
2013	May	0000	CCCCBBCCDA	AACCCABAA**A**	CBCCDDDDDX	31
		1200	CCDCACCDD**A**	BBCCCABABA	BBCDDDDDXX	31
	Jun	0000	XXCBCCXXCB	BBABCDDDXX	BDBCCXXXXD	30
		1200	XDBCCDXDCB	BABBDDDXXB	CBBCXXXXXD	30
2014	May	0000	CCBBBBCCCD	DCBD**A**BXBA**A**	ADDCDCCBBBC	31
		1200	CBDABCDCDD	CBDAAXBAA**A**	BDCCDBBABCD	31
	Jun	0000	XDACAABBBC	CTTTTTTDDB	DCBCCDXCAC	24
		1200	XACBAABBDC	TTTTTTTDBD	CCBCDXDBAC	23
Total			A+: 13, A: 61, B: 75, C: 88, D: 67, X: 46 (T: 29)			337

156 **Table 3: The full classification result for all the 24-h verification periods during the three mei-yu**
157 **seasons of 2012-2014. For each month, the first (second) row gives the results of 0000-2400 (1200-1200)**
158 **UTC. While the groups of A-D and X are denoted by their corresponding letter, a bold A indicates group A+ (a subset of A) and T marks the periods influenced by**
159 **tropical cyclones and thus excluded from study.**

160 **2.4 Categorical measures of model QPFs**

161 As mentioned, the 24-h QPFs by CReSS are verified against the rain gauge data, at three different ranges of 0-24, 24-

162 48, and 48-72 h (days 1-3). For this purpose, objective scores computed from the standard 2×2 contingency table (or

163 the categorical matrix) at a wide range of 14 thresholds from 0.05 to 750 mm are adopted. These measures include the

164 TS (also called critical success index), bias score (BS), probability of detection (POD), and false alarm ratio (FAR),

165 respectively defined as (e.g., Schaefer, 1990; Wilks, 2011; Ebert et al., 2003; Barnes et al., 2009)

166 $TS = H/(H + M + FA),$ (1)

167 $BS = (H + FA)/(H + M) = F/O,$ (2)

168 $POD = H/(H + M) = H/O,$ and (3)

169 $FAR = FA/(H + FA) = FA/F,$ (4)

170 where H, M, and FA are the counts of hits (both observed and predicted), misses (observed but not predicted), and

171 false alarms (predicted but not observed), respectively, among a total number of N verification points. Here, $N = H +$

172 $M + FA + CN$, where CN is the correct negatives (neither observed nor predicted), and the total counts in observation

173 (O) and forecast (F) are simply $O = H + M$ and $F = H + FA$. The values of TS, POD, and FAR are all bounded by 0

174 and 1, and the higher (lower) the better for TS and POD (FAR). For BS, its value can vary from 0 to ∞ (or $N - 1$ in

175 practice), but unity is the most ideal and implies no bias. Also, BS >(<) 1 implies overestimation (underestimation) of

176 the events. By interpolating the model QPFs onto the gauge sites that serve as verification points (i.e., $N \approx 440$ per

177 segment) using the bi-linear method, the counts of H, M, FA, and CN at any given threshold can be easily obtained

178 for each segment. Although the density of rain gauges varies to some extent (roughly every 5-10 km in the plains and

179 ≥10-20 km in the mountains, cf. Fig. 1b), their weights are assumed equal (e.g., Wang, 2014). For any group (e.g.,

180 A+) at a given threshold, the scores are obtained from a single 2×2 table that combines the entries from all segments,

181 so that the sample sizes are maximized (cf. Table 2, e.g., W15). This practice also remedies the issue of sampling in-

182 homogeneity and increases the stability of results, especially toward the high thresholds, as long as the points involved

183 in the matrix are not too few in number (cf. Table 2). Since neither the observation nor the forecast ever reached 750

184 mm (per 24 h) during the study period, results for 13 thresholds from 0.05 up to 500 mm (the next highest threshold)

185 are presented in later sections. Also, only 24-h QPFs are evaluated in the current study. Except for the categorical

186 matrix, subjective visual verification is also used in the selected examples (Section 4).

187
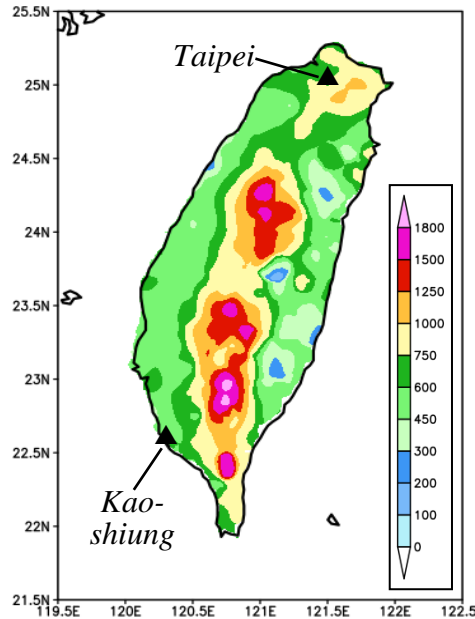
188 **Figure 3: Spatial distribution of mean total rainfall (mm) per mei-yu season (1 May through 30 Jun) in 2012-2014. The**
189 **cities of Taipei and Kaoshiung are marked.**

190 **3 Mei-yu QPFs in 2012-2014**

191 **3.1 Overall performance by the 2.5-km CReSS**

192 Following the method described above, the categorical matrices across the thresholds are obtained and the overall

193 ability of CReSS in mei-yu QPFs during 2012-2014 is shown in Fig. 4 using the performance diagram. Proposed by

194 Roebber (2009), the diagram uses the success ratio (SR = 1 − FAR = H/F) and POD as its two axes, and can also

195 depict the TS (gray curved isopleths, higher toward upper-right) and BS (brown dotted lines) simultaneously. In Fig.

196 4, the scores from forecasts at both 0000 and 1200 UTC for segments (of 24 h) in groups A+, A to D, and all periods

197 (A-D plus X, cf. Table 2) at 13 thresholds are shown for ranges of day 1, 2, and 3, respectively. The "all" group (black)

shows the overall accuracy for all mei-yu rainfall without classification, and its TS for day-1 QPFs decreases slowly from 0.6 at 0.05 mm to 0.18 at 100 mm, 0.15 at 250 mm, and 0.09 at 500 mm (Fig. 4a). Over heavy-rainfall thresholds ≥ 160 mm, the TSs of 0.09-0.16 are considerably higher than those reviewed in section 1. Even on day 2, the TSs remain at 0.11 to 0.06 over 160-500 mm, and above 0.03 up to 350 mm on day 3 (Figs. 4c,e).

When all segments are stratified by the observed event magnitude, the TSs are higher and the skill better for larger events than smaller ones, following the order of A+ then A to D for all thresholds at all three ranges without any exception (Fig. 4), while each individual curve mostly decreases with threshold when rain areas reduce in size (as shown in Fig. 5). Thus, the positive dependency of categorical measures on rainfall amount is also strong and evident in mei-yu QPFs in Taiwan, as predicted by W15. Linked to this dependency, the TSs for large events are also higher than those for the "all" group from the entire sample. For the most hazardous group A+, the TS on day 1 is 0.34 at 100 mm, 0.24 at 250 mm, and 0.16 at 500 mm (per 24 h, Fig. 4a). On days 2 and 3, the corresponding TSs are 0.32, 0.15, and 0.07 (Fig. 4c), and 0.25, 0.05, and 0.00 (Fig. 4e), respectively, all higher than their counterparts for the all group (except day 3 at 500 mm). Similar to some earlier studies (e.g., Chien et al., 2002, 2006; Chien and Jou, 2004; Yang et al., 2004), if we select TS ≥ 0.15 to indicate some level of accuracy, then the QPFs by the 2.5-km CReSS can reach it all the way up to 500 mm (per 24 h) on day 1, 250 mm on day 2, and 130 mm on day 3. Also, for A+, A, and all groups, the TSs of day-2 QPFs stay quite close to the values on day 1, and some are even identical, from low thresholds up to 200-250 mm. For day-3 QPFs compared to day 2, the same is true up to about 130 mm (Fig. 4, left column). Such results that some skill of heavy-rainfall QPFs still exists on days 2-3 are very encouraging. On the other hand, at thresholds ≥ 50 mm, the model's ability for B-D events (Fig. 4, right column) are limited (TS ≤ 0.08) when the rain areas are relatively small (with O/N ≤ 6%, Fig. 5), but as discussed in W15, this is not important due to low hazard potential.

Another fairly subtle but important feature in Fig. 4 is that the TSs of all, A, and A+ groups decrease only marginally for some heavy-rainfall thresholds, particularly on days 1-2, despite the reduction in rain-area size (left column). Some examples include the TSs for group A+ over 100-350 mm on day 1 (drops from 0.34 to 0.21), and those for group A over the same thresholds on day 1 (from 0.23 to 0.15) and over 100-250 mm on day 2 (from 0.20 to 0.14). Even on day 3, the decrease of A and "all" curves from 160 to 350 mm is rather slow, although the TSs there are only 0.03-0.07 (Fig. 4e). Such a slow decline in TSs with thresholds indicates that in a relative sense, the model is more capable to produce hits toward the rainfall maxima, which occur more frequently in the mountains (cf. Figs. 1b and 3).

By definition, both POD and SR cannot be lower than the TS [cf. Eqs. (1), (3), and (4)], and the ratio of POD/SR equals to the BS (thus, POD < SR if BS < 1 and vice versa). In Fig. 4, the PODs start at 0.05 mm from nearly perfect values of 0.98-0.99 for days 1-3 for group A+, at least 0.9 for A, and ≥ 0.72 for all segments (left column). For these three groups, the PODs at 250 mm remain at least 0.32 on day 1, 0.21 on day 2, and 0.05 on day 3. Like the TS, the POD for mei-yu rainfall indeed decreases quite significantly with forecast range (lead time), particularly toward high thresholds, mainly due to error growth and the reduction in predictability. However, even on day 3, POD and TS can still reach 0.16 and 0.07 at 130 mm (for all segments), respectively. The SR values (and thus FAR) are again the best for group A+ and ≥ 0.36 across all thresholds on day 1, including 500 mm (Fig. 4a). On day 2, the SRs for A+ over 130-500 mm decrease but not by too much, and the values over 10-250 mm even increase on day 3 (Figs. 4c,e). Often,

235   the SR for A+ is considerably higher than those for A and all events regardless of forecast range, particularly over

236   heavy-rainfall thresholds. Overall, the model also produces higher POD and SR (i.e., lower FAR) for larger events

237   compared to smaller ones at all thresholds and all three forecast ranges in Fig. 4, with only a few exceptions after close

238   inspection. This indicates that the high-resolution CReSS not only produces larger rainfall for large rainfall events,

239   which leads to a higher TSs, but also produces larger rainfall for small events, which leads to lower SR values. In

240   summary, as for typhoon rainfall (W15), the 2.5-km CReSS is the most skillful in predicting the largest events in the

241   mei-yu season in Taiwan..

242   Next, the BS values are examined for over/under-prediction (i.e., above/below the diagonal line) in Fig. 4, where the

243   threshold with O/N falling below 1% is marked to indicate values that might be potentially unstable and less

244   meaningful. For day-1 QPFs, the BSs for all segments suggest slight under-prediction for low thresholds $\leq$ 10 mm

245   (per 24 h), but some over-prediction (BS $\approx$ 1.25-1.5) across 50-350 mm (Fig. 4a). On the contrary, the model shows

246   slight over-prediction over 0.05-75 mm for the largest events of group A+ (with BSs up to 1.15), but under-prediction

247   toward higher thresholds, with the lowest BS of 0.52 at 350 mm. Mostly between the two curves mentioned above,

248   the curve for group A stays closer to unity and is more ideal across nearly all thresholds (Fig. 4a). For B-D groups

249   (Fig. 4b), their characteristics are similar to the All group, with BSs of 0.8-1.0 at low thresholds but generally some

250   over-prediction across higher thresholds. However, their BS values rarely exceed 2.5, unless the O/N values drop to

251   below 1%. The situation for BSs between different groups remains similar on days 2 and 3 (Figs. 4c-f), and the over-

252   forecasting across the middle thresholds in group A (at all ranges) can be confirmed to come mainly from groups B-

253   D, as groups A+ and A exhibit little or a much less tendency for over-prediction there (Fig. 4).

254   Toward the longer ranges of days 2 and 3, the BS values in general become smaller, particularly for the larger groups

255   (Fig. 4, left column). Thus, the over-prediction in group A is reduced and the under-prediction in A+, which is the

256   most important group, becomes more evident, especially toward the high thresholds (Figs. 4c,e). For example, the BS

257   of day-2 QPFs for A+ is ideal and $\geq$ 0.8 up to 200 mm but declines to about 0.35 at 500 mm, but it is already below

258   0.4 at 130 mm on day 3. This indicates that for larger events, the error growth with lead time in the model tends to

259   become less rainy, as reflected in the decrease in BS. Thus, the probability to under-forecast peak rainfall rises with

260   lead time. For smaller events that do not produce much rainfall (i.e., B-D and X), a similar tendency does not exist or

261   is weaker, and BS tends to be greater than unity. So, to say the least, one needs to practice caution in the interpretation

262   of BS, which can also become unstable when O/N approaches zero (which inevitably happens at certain thresholds).

263
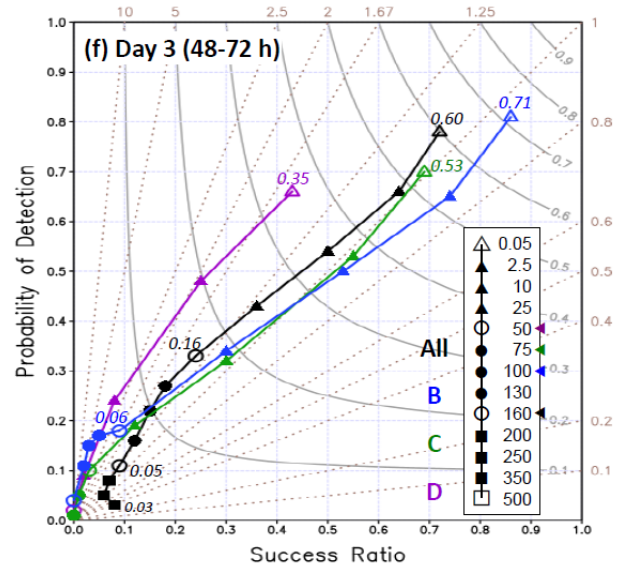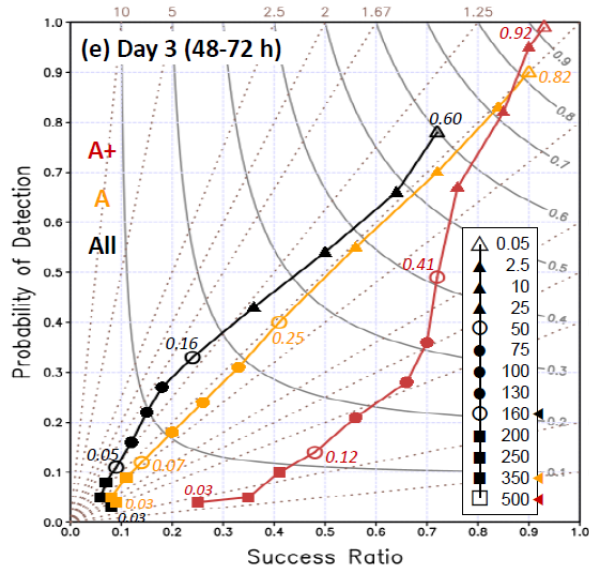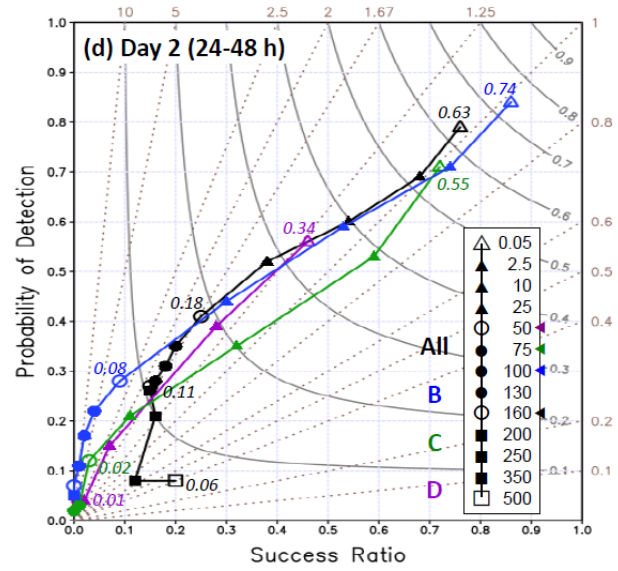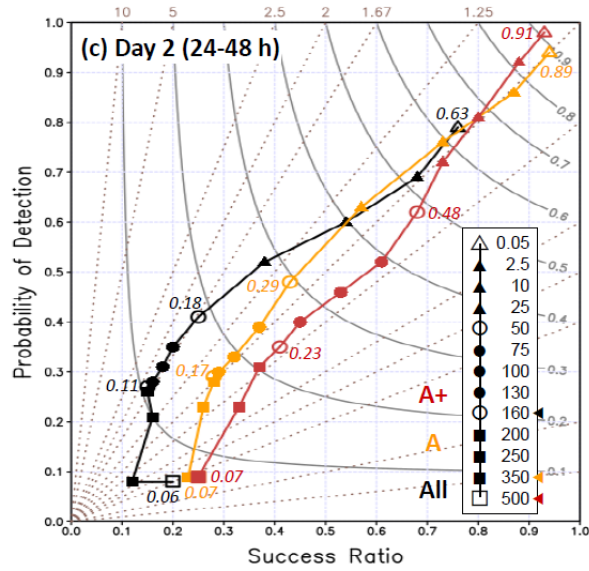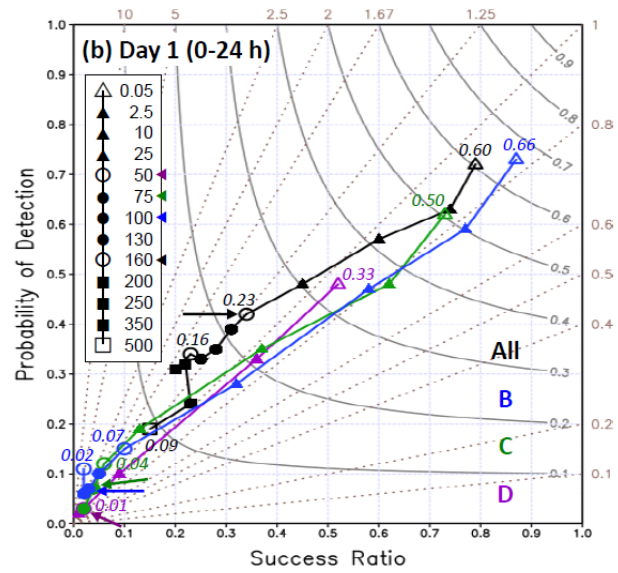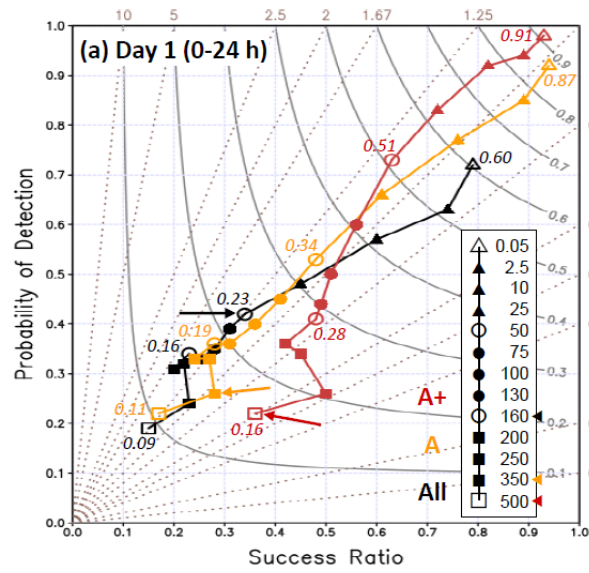
Figure 4: Performance diagrams of 24-h QPFs for (a),(b) day 1 (0-24 h), (c),(d) day 2 (24-48 h), and (e),(f) day 3 (48-72 h) by the 2.5-km CReSS, at 13 rainfall thresholds (inserts) from 0.05 to 500 mm, during three mei-yu seasons (May-Jun) in 2012-2014 in Taiwan. Results for groups A+, A, and All (All, B, C, and D) are plotted in left (right) column with different colors. TS values are labelled at fixed thresholds of 0.05, 50, 160, and 500 mm (open symbols) or selected endpoints (smaller fonts), and data points with TS = 0 at high thresholds are omitted. For each group, the threshold where the observed rain-area size (*O/N*) falls below 1% is labeled in insert, and also marked by an arrow in (a),(b).

3.2 Improvement in heavy-rainfall QPFs

To assess the improvement in heavy-rainfall QPFs in mei-yu season, our results in Fig. 4 are compared to Fig. 2 and those reviewed in Section 1. However, the differences in model resolution should be noted. Overall, the "all" curves in Fig. 4 indicate that the 2.5-km CReSS exhibits better skill than those reviewed in Section 1 (with Δx as fine as 5 km at most), especially at thresholds above 100 mm (e.g., TS = 0.15 at 250 mm and 0.09 at 500 mm for day 1). With even higher TSs for larger and more hazardous events (groups A and A+), the improvement of heavy-rainfall QPFs in the present study from earlier results is therefore quite clear and dramatic. The physical explanation will be further elaborated and discussed later in Section 4.
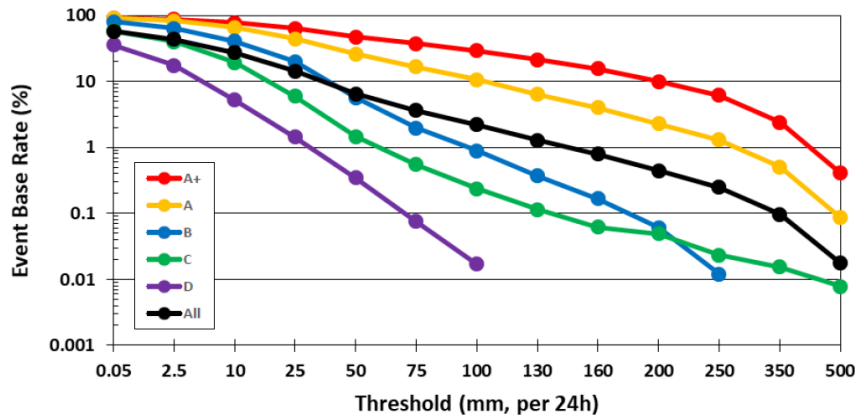
Figure 5: Observed rain-area size or base rate (*O/N*, %) of 24-h rainfall (same for days 1-3) in logarithmic scale used to compute the scores in Fig. 4

4 Examples of Model QPFs

Given the success of the CRM in its overall performance, some examples of CReSS forecasts are selected and presented in this section. The main goal here is two-fold: 1) To illustrate how the model behaves and captures the rainfall in individual forecasts, and thus 2) to identify where such a CRM has a better capability in QPFs and where it has limitations in Taiwan. Since our focus is on heavy rainfall, the event during 9-12 June 2012, the largest during our study period, is chosen for illustration.

The event of 9-12 June 2012 spanned four days and contributes more than half the segments in group A+ (7 in 13, cf. Table 3). In Fig. 6a, the observed 24-h rainfall distributions over Taiwan are shown every 12 h, from 1200-1200 UTC 8 June to 0000-2400 UTC 12 June 2012. Except for the first forecast period, all seven segments are qualified as A+ and five have a 24-h peak rainfall over 500 mm (those since 1200 UTC 9 June). Three rainfall maxima from this lengthy event exist: over southern CMR, near the intersection of CMR and SMR in central Taiwan, and over northern Taiwan (Fig. 6a). The rain at the two mountain centers (cf. Fig. 1b) is much more persistent than that in northern

Taiwan, which concentrated mainly over a 10-h period beginning 1400 UTC 11 June (Wang et al., 2016b). The southwestern plains also received considerable rainfall, especially around 9 June (Fig. 6a).
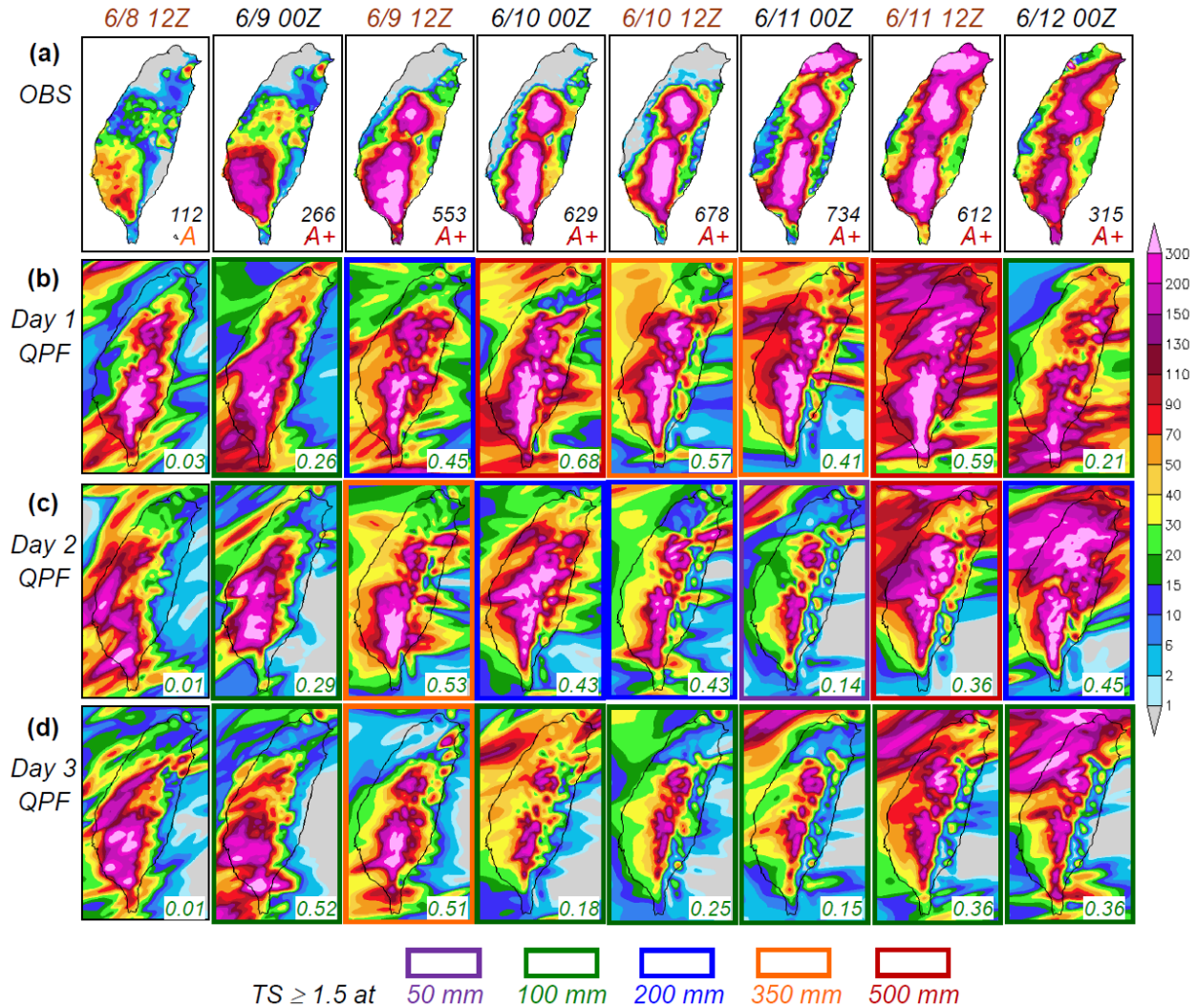
Figure 6: (a) The observed 24-h accumulated rainfall (mm, scale on the right) over Taiwan from 1200 UTC 8 Jun to 0000 UTC 13 Jun 2012, given every 12 h (from left to right), with the beginning time of accumulation (UTC) labeled on top (black for 0000-2400 UTC and brown for 1200-1200 UTC). (b) Day-1 (0-24 h), (c) day-2 (24-48 h), and (d) day-3 (48-72 h) QPFs valid for the same 24-h periods as shown in (a) by the 2.5-km CReSS (starting at 0000/1200 UTC under black/brown headings). In (a), peak 24-h rainfall (mm) and classification group are labeled. In (b)-(d), thick boxes in purple, green, blue, orange, and scarlet denote forecasts having a TS ≥ 0.15 at the threshold of 50, 100, 200, 350, and 500 mm (per 24 h), respectively, and the TS at 100 mm is also given (lower right corner).

The 24-h QPFs produced by the 2.5-km CReSS (at 0000 or 1200 UTC) in real time targeting the same periods as in Fig. 6a, at the ranges of days 1-3 are presented in Figs. 6b-d, with the general quality expressed by the TS at 100 mm (lower right corner inside panels) and thickened outline for TS ≥ 0.15 at the threshold of 50, 100, 200, 350, or 500 mm. The day-1 QPFs (Fig. 6b) are made from the forecasts starting (with initial time t_0) at the time of the heading, while day-2 (Fig. 6c) and day-3 QPFs (Fig. 6d) are those made 24 and 48 h earlier (for the same target period), respectively. In Fig. 6, this extreme and long-lasting event was generally well captured by the model, especially on

310   day 1 where the overall rainfall pattern and TS both tend to be better, as expected. The best day-1 QPF is for 0000-

311   2400 UTC 10 June (TS = 0.68 at 100 mm and 0.40 at 500 mm), followed by the one for 1200 UTC 11-12 June (TS =

312   0.59 at 100 mm and 0.29 at 500 mm, columns 4 and 7, Fig. 6b). At longer ranges on days 2 and 3, the rainfall

313   magnitudes produced over the mountains and southwestern plains are also comparable to observations, but the event

314   starts somewhat earlier and becomes less rainy during 10-11 June showing under-forecast (Figs. 6c,d). As a result, the

315   TSs for the segments starting at 1200 UTC 8 June and during 10-11 June (columns 1 and 4-7) mostly increase from

316   longer to shorter ranges, i.e., with better QPFs at later times. This relationship with range does not hold true for the

317   other segments, among which the day-3 and day-2 QPFs for the period of 1200 UTC 9-10 June (TS ≥ 0.51-0.53 at

318   100 mm and 0.20-0.31 at 350 mm) and the day-2 QPF for 1200 UTC 11-12 June (TS = 0.40 at 500 mm) are particularly

319   impressive (columns 3 and 7). Compared to the rain over the terrain, the maximum across Taipei in northern Taiwan

320   during 11-12 June was largely over lower and flatter regions (cf. Figs. 1b and 2) and more challenging for the model

321   to predict at the right location (Fig. 6), an aspect that will be further elaborated on later. Note, nevertheless, that since

322   the mountain regions are the only places where rainfall amounts reach 300 mm in both the observations and the model

323   (Fig. 6), any hits at and above this threshold occur in the mountains.

324   Figure 7 shows the TS and BS of day-1 to day-3 QPFs from the runs made at a series of initial times, including 1200

325   UTC of 7-9 June and the next four from 0000 UTC 10 to 1200 UTC 11 June (top to bottom), and our focus is mainly

326   over the thresholds ≥ 100 mm. Inside the panels, the observed event base rate (O/N, i.e., rain-area size, identical at the

327   same threshold for the same target period) and the hit probability (H/N, note that $H/N \leq O/N$) are given at selected

328   points. Figures 7a-7f provide some examples on how the model did in predicting the beginning of the event (cf. Fig.

329   6, columns 1-3). As mentioned, the day-3 QPF made from 1200 UTC 7 June (Figs. 7a,b, blue curves) and day-2 QPF

330   made one day later (Figs. 7c,d, red curves), both targeting 1200 UTC 9-10 June, are of fairly high quality. With rain

331   areas (O/N) occupying 31%, 14%, and just 2% of Taiwan at 100, 200, and 350 mm, the day-2 QPF in Fig. 7c, with

332   BS ≈ 0.6-1.1 (Fig. 7d), yields TSs of 0.53-0.31 at these thresholds. The day-3 QPF with t_0 at 1200 UTC 7 June, with

333   less predicted rain and BS ≈ 0.3-0.6 (cf. Fig. 6d, column 3), the TSs are 0.51-0.2 (Figs. 7a,b). With TS at least 0.2 at

334   350 mm (an amount predicted only in southern CMR), both QPFs (for 1200 UTC 9-10 June) are quite good. Valid for

335   periods with varying magnitude (B, A, and A+), the forecasts in Figs. 7a,b are also good examples to illustrate the

336   dependency property (Fig. 4 and W15), where the rainfall amount apparently exhibits a larger influence on the scores

337   than the forecast range. In Figs. 7e,f, the TS curves at the three ranges (all for A+ events) are closer.

338   In Fig. 8, the actual forecast near Taiwan between 42 and 69 h, from the run made at 1200 UTC 7 June, is compared

339   with radar observations every 6 h to examine general rainfall locations. While a wind-shift line existed off eastern

340   Taiwan, the surface mei-yu front was well to the north with prefrontal low-level southwesterly flow impinging on the

341   island during this period (also Wang et al. 2016b). Active convection constantly developed over the mountains in

342   central and southern Taiwan and moved from the upstream ocean into the southwestern plains, and this scenario was

343   well captured by the 2.5-km CReSS (Fig. 8), yielding a high-quality QPF on day 3 despite some under-forecast at

344   thresholds ≥ 75 mm (cf. Figs. 7a,b).

345
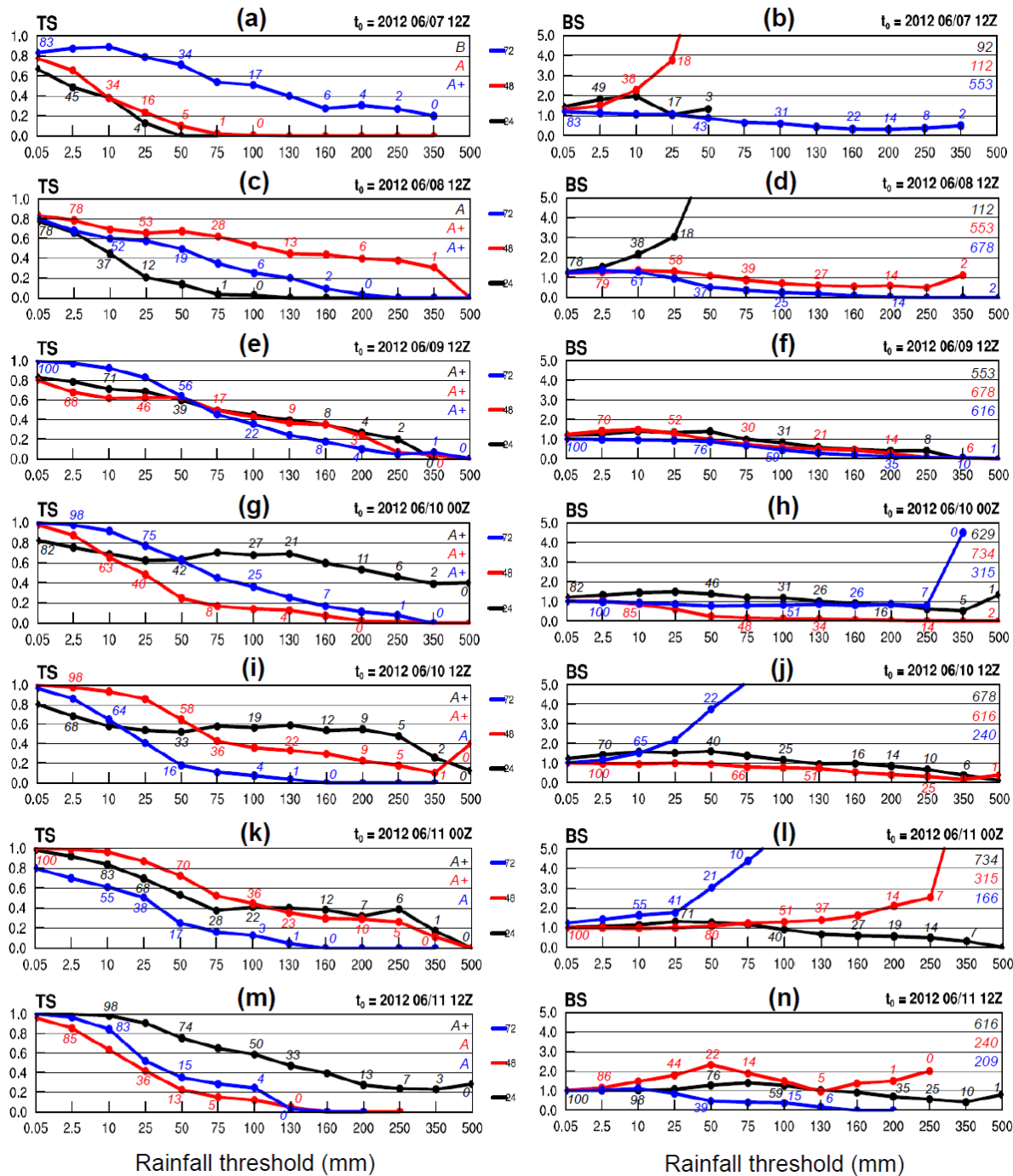
Figure 7: (a) TS and (b) BS of day-1 (black), day-2 (red), and day-3 (blue) QPFs made at 1200 UTC 7 Jun 2012 as a function of rainfall threshold (mm, per 24 h). The hit rate (*H/N*, %, rounded to integer) at selected points and the classification group for each day are labeled in the left panel (for TS). The observed base rate (*O/N*, %) and peak 24-h rainfall (mm) are labeled in the right panel (for BS). (c),(d) to (m),(n) As in (a),(b), except for the QPFs made at (c),(d) 1200 UTC 8 Jun, (e),(f) 1200 UTC 9 Jun, (g),(h) 0000 and (i),(j) 1200 UTC 10 Jun, and (k),(l) 0000 and (m),(n) 1200 UTC 11 Jun, 2012, respectively.

In the four following forecasts made on 10-11 June (Figs. 7g-n), the dependency on event magnitude exists, but the QPFs made for A+ periods tend to have higher TSs above 75-100 mm at the shorter ranges (Figs. 7g,i,k). The TSs of these day-1 QPFs can be as high as 0.48 at 250 mm and 0.40 at 500 mm. At 350-500 mm, such high TS occurs with *O/N* below < 10% (or even only 1%), and thus indicates remarkable model accuracy in predicting the peak rainfall at

355   the correct location in the mountains in this event. Over thresholds ≥ 200 mm, BS values in Fig. 7 indicate that under-

356   prediction for this extreme event occurs much more often than over-prediction, while they also tend to be closer to

357   unity (with less under-forecast) for QPFs achieving higher TSs. Consistent with Fig. 4, an over-prediction is more

358   likely to happen for smaller events (A or below), across low thresholds below 50 mm, and/or when the rain area

359   becomes small. In Fig. 7, for example, BS ≥ 2 at high thresholds for A+ group occurs only when O/N approaches zero

360   (Figs. 7h,n), with the only exception in Fig. 7l on day 2. Overall, the model does not have a tendency to over-predict

361   such a large event (cf. Fig. 6).

362
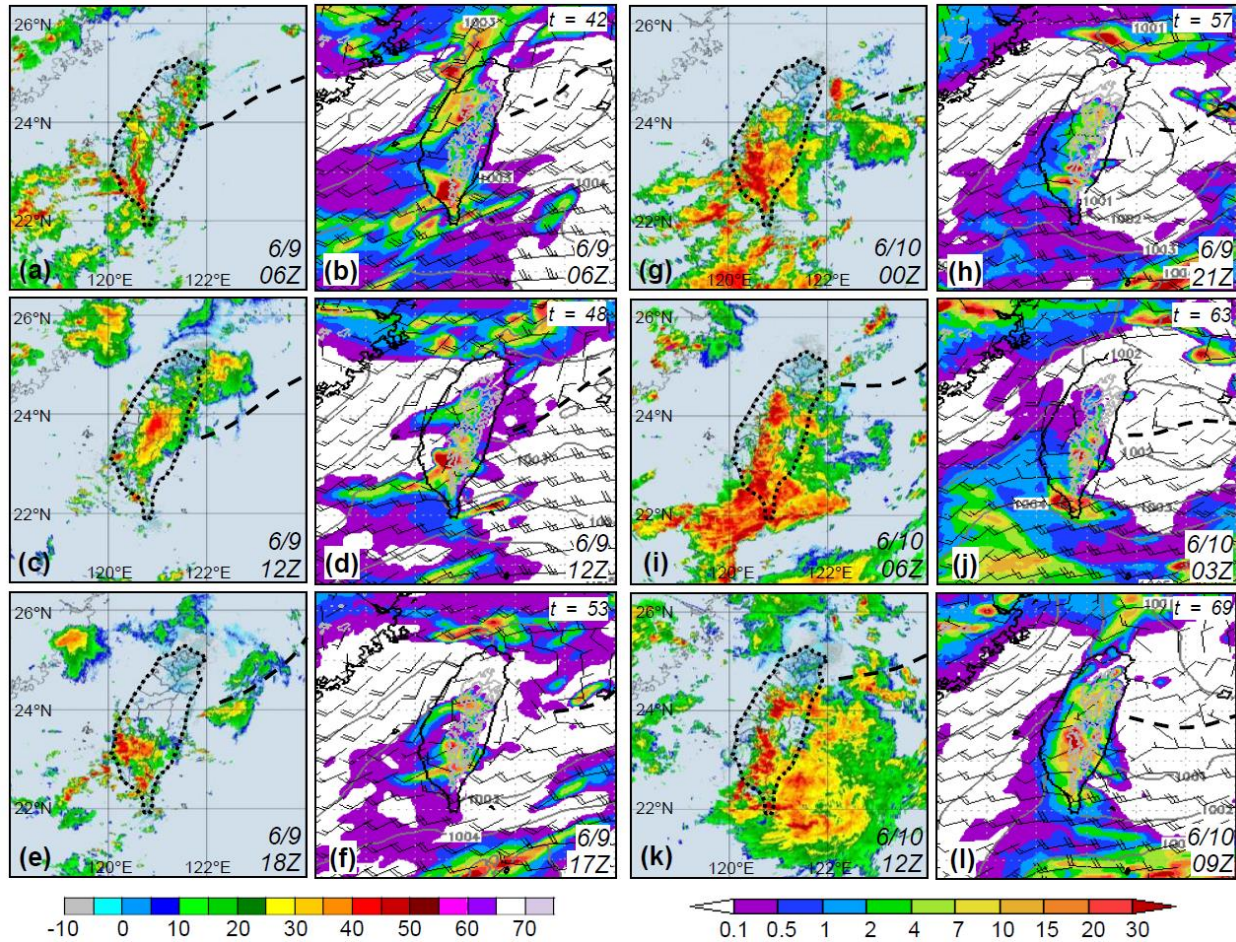
Figure 8: (First and third column) Radar reflectivity composite (dBZ, scale at bottom left) in the Taiwan area (width roughly 600 km) every 6 h from (a) 0600 UTC 9 Jun to (k) 1200 UTC 10 Jun, 2012 (original plots provided by the CWB). (Second and fourth column) The CReSS forecast, starting from 1200 UTC 7 Jun 2012, of sea-level pressure (hPa, every 1 hPa, over ocean only), surface wind (kts, barbs, at 10 m), terrain height at 1 and 2 km (gray contours), and hourly rainfall (mm, color, scale at bottom right) valid at the time or within 3 h of the radar composite as labeled [in UTC (forecast time in h) at lower (upper) right corner] over the same area. The thick dashed lines mark the position of surface frontal or wind-shift line, based on NCEP gridded analyses for the observation (outline of Taiwan also highlighted).

370   The forecasts on days 1-2 produced by the run starting at 1200 UTC 10 June are compared with radar observations in

371   Fig. 9. Together with Fig. 8, the radar panels cover the wettest 72 h (0600 UTC 9-12 June) of the entire event. During

372   day 1 (Figs. 9a-h), the scenario remains similar to Fig. 8, and the model again was able to capture the mountain rainfall.

373   The convection moving in from the Taiwan Strait, however, was too active and the rain along the western coast on

374   day 1 was over-predicted with BSs ≈ 1.2-1.6 from 0.05 up to 100 mm (cf. Fig. 7j). Note that in Fig. 7, some over-

375   prediction across low thresholds can also exist for group A+ and lowers the TS, which otherwise can often exceed 0.8

376   at and below 25 mm. In any case, the model's performance over the low thresholds is of secondary importance.

377   Since 1200 UTC 11 June, the mei-yu front gradually approached northern Taiwan, and its western section moved

378   rapidly across the island after about 0000 UTC 12 June (Figs. 9i-p). Studied by Wang et al. (2016b), the heavy rainfall

379   in northern Taiwan (during 1400-2400 UTC) was caused by quasi-linear convection that developed south of the front

380   (Figs. 9i,k,m), along a convergence zone between the low-level flow blocked and deflected by Taiwan's topography,

381   and unblocked flow further to the northwest (but still prefrontal) in the environment (also e.g., Li and Chen, 1998;

382   Yeh and Chen, 2002; Chen et al., 2005; Wang et al., 2005). In the model forecast, with apparent errors in the position

383   and moving speed of the front (Figs. 9i-p), it is highly challenging to produce a similar system at the correct location

384   and time even when the overall scenario surrounding northern Taiwan are reasonably predicted. In the simulation of

385   Wang et al. (2016b), the rainbands cannot be fully captured even with a finer grid of $\Delta x = 1.5$ km and the NCEP final

386   analyses as IC/BCs. Likely mainly linked to the IC/BCs, the position error of the front in this case is still a major error

387   source for the rainfall associated with the front. Thus, although the model did indicate a real possibility of heavy

388   rainfall in northern Taiwan in Fig. 9, the high TS of 0.4 at 500 mm on day 2 (Fig. 7i) came from the mountains, where

389   the rainfall prediction is clearly more accurate (cf. Figs. 6a,c, column 7), consistent with Walser and Schär (2004). Of

390   course, the day-1 QPF with $t_0 = 1200$ UTC 11 June performed better in northern Taiwan than our example, but the

391   goal here is to illustrate the relatively high accuracy to predict heavy rainfall phase-locked to the topography versus

392   the low accuracy for rainfall produced by transient systems over low-lying plains.

393   The above example, together with other cases including those on 20 May 2013 and 20-21 May 2014, (cf. Table 3, not

394   shown), suggests a lower accuracy and a more challenging task for model QPFs to capture the heavy rainfall produced

395   by transient systems often in close association with the mei-yu front, compared to topographic rainfall in Taiwan.

396   Even though the overall scenario is reasonably and realistically predicted (cf. Figs. 8 and 9), some position errors on

397   the mei-yu front are almost inevitable and the intrinsic predictability can limit the accuracy of the QPF (e.g., Hochman

398   et al., 2021). Also, for such rainfall caused by transient systems, categorical statistics are known to be less effective in

399   verifying model QPFs (e.g., Davis et al., 2006; Wernli et al., 2008; Gilleland et al., 2010). However, for the quasi-

400   stationary, phase-locked rainfall over the topography in the majority of large events (in both mei-yu and typhoon

401   seasons, e.g., Chang et al., 1993; Cheung et al., 2008) in Taiwan, they are still valid and useful as shown herein. As

402   model resolution increases, both the topography and deep convection can be better resolved, leading to improved

403   QPFs over the terrain.
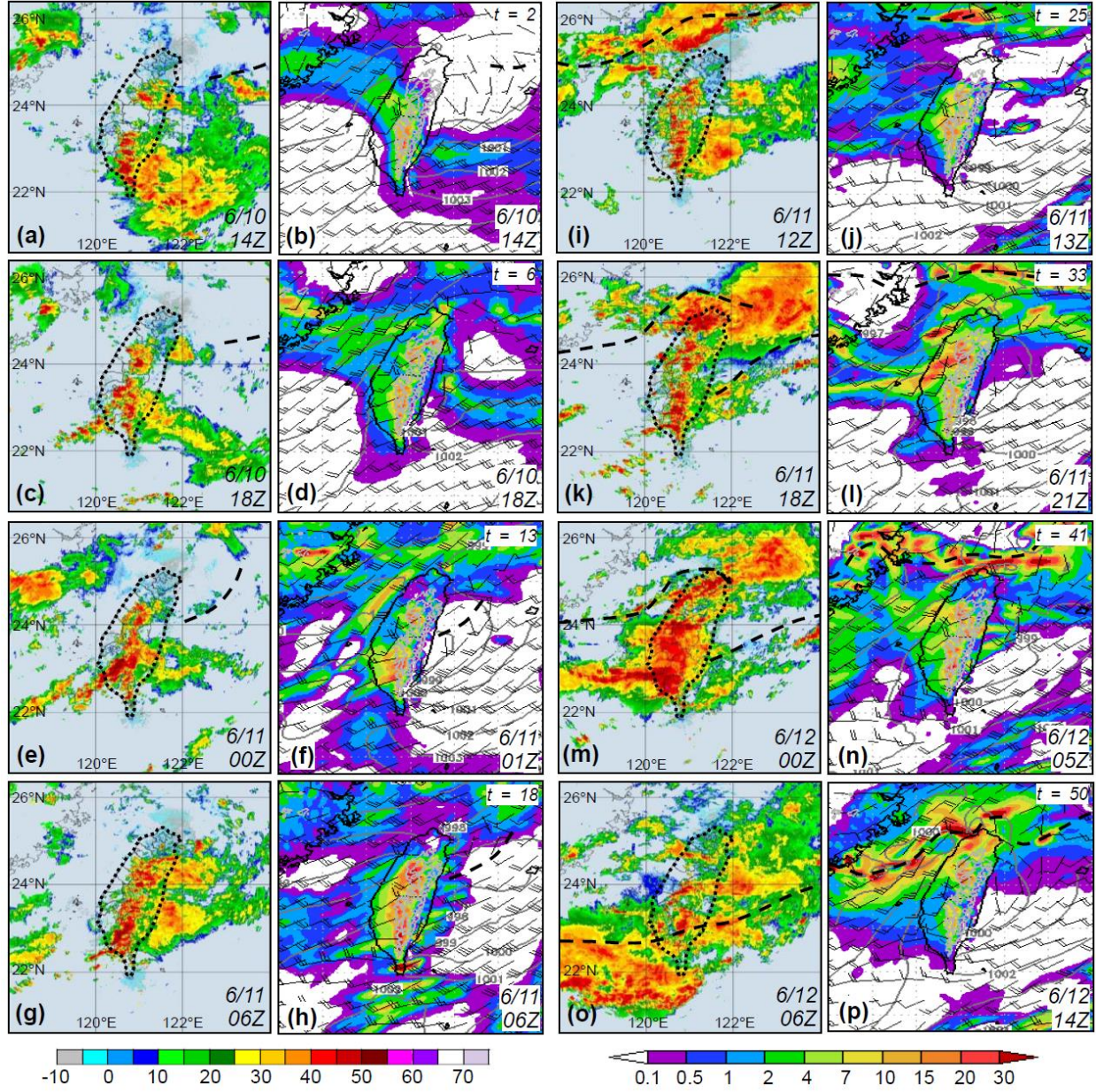
Figure 9: As in Fig. 8, but showing (columns 1 and 3) radar reflectivity composite (dBZ) at (a) 1400 UTC 10 Jun and every 6 h from (c) 1800 UTC 10 Jun to (o) 0600 UTC 12 Jun, 2012, and (columns 2 and 4) the CReSS forecast, starting from 1200 UTC 10 Jun 2012, of sea-level pressure (hPa), surface wind (kts), and hourly rainfall (mm) valid at the time or within up to 8 h (towards the end) of the radar composite (as labeled).

5 Dependency of Categorical Scores to Event Size

In Section 3, a positive dependency in categorical measures by CReSS, including TS, POD, and FAR, on rainfall amount is shown for the mei-yu regime in Taiwan, as predicted. Also discussed in W15, this property arises mainly due to the positive correlation between the scores and rain-area sizes, as illustrated in Fig. 10 with a correlation coefficient $r = 0.89$ for the mei-yu regime. However, to explore whether the model is indeed more skillful in predicting

414 larger rainfall events, further analysis with the factor of rain-area size removed is needed. Different from W15, our

415 approach here is described below.

416 For each segment, the statistics (*H*, *M*, *FA*, and *CN*) at 13 fixed thresholds of 0.05-500 mm, each occurring at a certain

417 *O/N* (if the threshold ≤ the observed peak amount), are known. The observed base rate (0-100%) is divided into bins

418 every 5% except at 0-5%, where it is subdivided into 0-0.5, 0.5-2, and 2-5% to give more comparable sample size.

419 For each group (A+ or A-D), the statistics are then summed for each bin regardless of their rainfall threshold. Thus,

420 those in the same bin come from rain areas with similar sizes. In Fig. 11a, the distribution of total counts of thresholds

421 across *O/N* is plotted, and the larger events toward A+ are more capable to produce rain areas larger in size (say, ≥60%

422 of Taiwan). Also, the counts remain mostly around 50 for *O/N* ≥ 40%, then rise to 200-300 with *O/N* ≤ 10%.

423
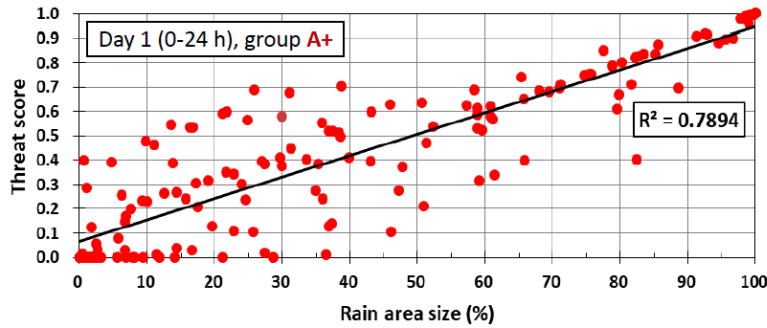
424 **Figure 10: Scatter plot of TS versus observed rain-area size (%) from day-1 QPFs for group A+ from 0% to 100% (from**
425 **high to low rainfall threshold). The square of correlation coefficient (R^2) is given.**

426 Due to fewer samples at larger *O/N* values, the TSs for different groups (from a single 2×2 table for each bin) are

427 presented only for *O/N* ≤ 40% in Figs. 11b-d. While the scores for B-D are roughly the same, the TSs for A are clearly

428 higher compared to them on day 1, and those for A+ are again higher compared to A on days 1 and 2 over most part

429 of this range, sometimes by 0.05-0.1, when the factor of rain-area size is removed (Figs. 11b,c). On day 3 (Fig. 11d),

430 however, the TSs for larger events (A+ and A) show no particular advantage. Therefore, similar to typhoons in W15,

431 the 2.5-km CReSS is more skillful in predicting the larger mei-yu events in Taiwan within 2 days, over the heavy-

432 rainfall area (again, mainly over the mountains).

433 The higher TSs and better skill for large events at *O/N* within 40% (Fig. 11) are most likely linked to the more favorable

434 conditions at synoptic to meso-α scale, which the model is capable to capture with higher accuracy (e.g., Walser and

435 Schär, 2004). To briefly elaborate on this aspect, seven items on the checklist used by CWB forecasters in the mei-yu

436 season as a guidance to issue heavy-rainfall warning (e.g., Wang et al., 2012a) are selected, and their occurrence

437 frequency, judged using surface weather maps and NCEP gridded analyses at the starting time of each 24-h periods

438 are compiled for different groups. These items include: 1) presence of surface mei-yu front inside 20°-28°N, 118°-

439 124°E; 2) Taipei (cf. Fig. 3) within 200 km south and 100 km north of the front; 3) Kaoshiung (cf. Fig. 3) within 200

440 km south of the front; 4) presence of low-level jet (LLJ) inside 18°-26°N, 115°-125°E at 850 or 700 hPa; 5) presence

441 of mesolow near Taiwan; 6) Taiwan inside a low pressure zone; and 7) the mean sea-level pressure in Taiwan is below

442 1005 hPa. The results (Fig. 12) indicate that among the seven items, an average of 4.15 items are met in group A+,

443 and this figure gradually declines toward smaller groups, from 3.67 in A, 2.84 in B, and finally to only 0.87 in X.

444 Thus, as expected, the synoptic and meso-α-scale conditions tend to be more favorable in larger events, which in

445 general also correspond to higher TS values (Figs. 3 and 11) in combination with the orographic forcing in Taiwan.

446
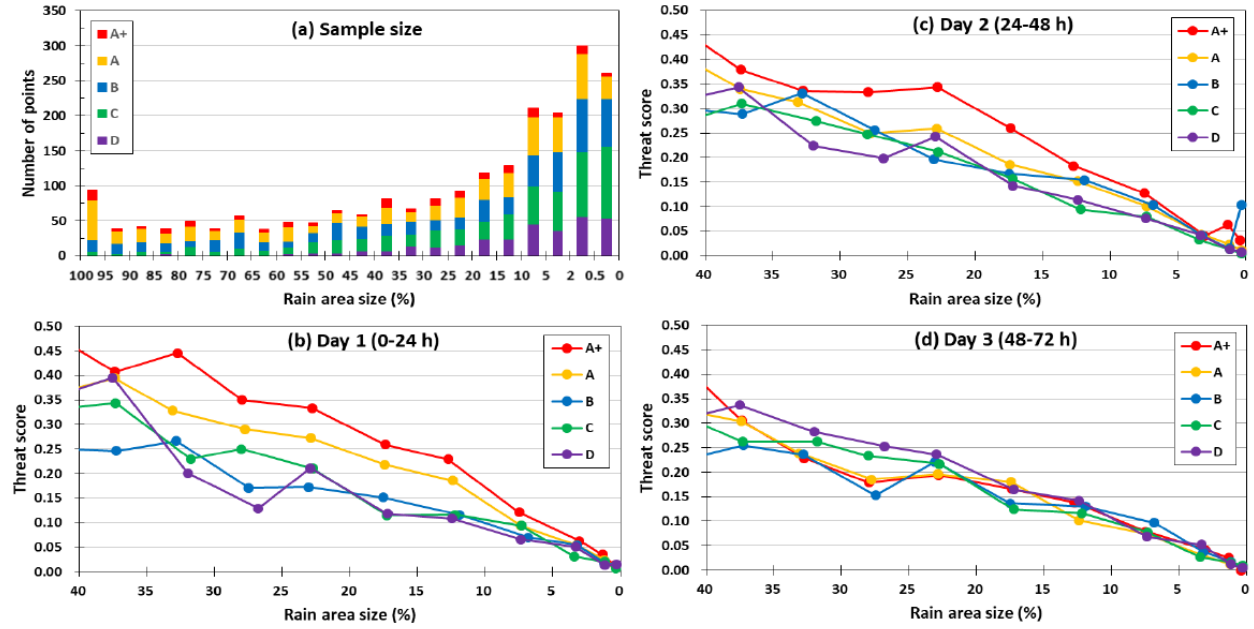
Figure 11: (a) The distribution of data points in the bins of observed rain-area size (%, every 5% from 100% to 5%, then

448 **2-5%, 0.5-2%, and < 0.5%; same for days 1-3) among groups A+ and A to D. (b)-(d) The TS of 24-h QPFs for (b) day 1 to**

449 **(d) day 3, respectively, as a function of observed rain-area size between 40% and 0%.**

450
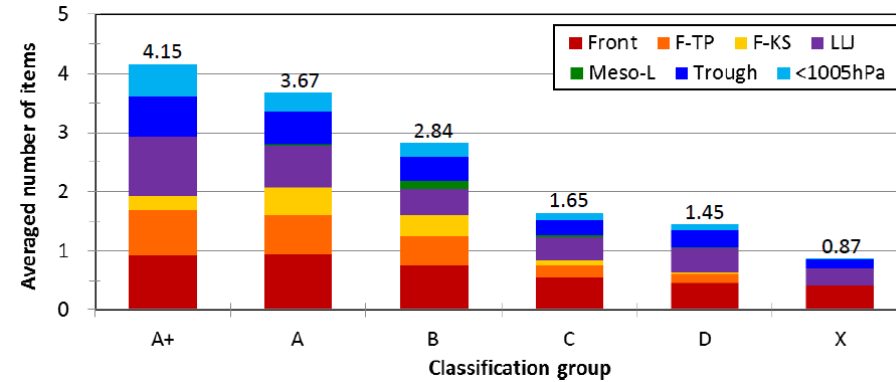
451 Figure 12: The average number of items met, among the seven items on the checklist, at the starting time of 24-h segments
452 for different classification groups (from A+, A to D, and X), with the value labeled on top. Following the order (bottom to
453 top), the seven items are: presence of surface mei-yu front (front), front near Taipei (F-TP), front near Kaoshiung (F-KS),
454 presence of LLJ, mesolow (meso-L), Taiwan inside a low pressure zone (trough), and the mean sea-level pressure lower
455 than 1005 hPa (<1005 hPa), respectively. The items are plotted in different colors (see insert) to show their proportion.

6 Summary and Concluding Remarks

457 In this study, the QPFs at the ranges of 1-3 days by the 2.5-km CReSS during three mei-yu seasons (May-June) in

458 Taiwan of 2012-2014 are evaluated using categorical statistics, with an emphasis on heavy to extreme rainfall events

459 (100-500 mm per 24 h). Overall, the TSs of day-1 QPFs for all events (no classification) at thresholds of 100, 250,

460 and 500 mm are 0.18, 0.15 and 0.09, respectively. Compared to previous and contemporary results from models at

461 lower resolutions for mei-yu season in Taiwan, where the TSs are no higher than 0.1 at 100 mm and approach zero at
462 200-250 mm and beyond (Section 1, e.g., Hsu et al., 2014; Li and Hong, 2014; Su et al., 2016; Huang et al., 2016),
463 the results herein show significant improvements by the 2.5-km CReSS, especially over the heavy-rainfall thresholds.
464 Moreover, the ability to represent the extreme and top events (group A+) in terms of the TS are much higher when a
465 proper classification based on observed rain area size (i.e., event magnitude) is used. For the top 4% and most
466 hazardous mei-yu events, the day-1 QPFs have TSs of 0.34, 0.24, and 0.16, respectively. The QPFs for larger events
467 also exhbit higher POD, lower FAR, and higher TS than smaller ones, across nearly all thresholds at all ranges of days
468 1-3. Thus, the positive dependency in categorical scores on the overall rainfall amount also exists in mei-yu regime in
469 Taiwan, as predicted by W15 (and Wang, 2016).

470 For a selected case study, the improvement by the 2.5-km CReSS in Taiwan is shown to lie in an improved ability to
471 capture the phase-locked topographic rainfall at its correct location in larger events at heavy-rainfall thresholds. For
472 rainfall in the mountains, the QPFs tend to be more accurate as the CRM can better resolve both the terrain and
473 convection (e.g., also Walser and Schär, 2004; Roberts and Lean, 2007). In contrast, the accuracy of QPFs for
474 concentrated rainfall caused by transient systems (such as frontal squall lines) could not be demonstrated probably
475 due to the difficulty to predict at the correct time and location owing to nonlinearity, even though a realistic scenario
476 is produced. Overall, the high-resolution models showed a higher QPF accuracy in categorical statics for extreme
477 events than coarser resolution models over the geographic region of Taiwan as demonstrated here (and in W15). Such
478 QPFs can be helpful to hazard preparation and mitigation.

Code and data availability

480 The model used in this study is called Cloud-Resloving Storm Simulator and its website for downloading model and
481 user's guide is at http://www.rain.hyarc.nagoya-u.ac.jp/~tsuboki/cress_html/index_cress_eng.html. And the rainfall
482 figures of Model is at the website http://cressfcst.es.ntnu.edu.tw/.

Author contribution

484 Chung-Chieh Wang designed the experiments and Pi-Yu Chuang carried them out. Chih-Sheng Chang operated the
485 real-time model forecasting and Kazuhisa Tsuboki created the model code. Shin-Yi Huang helped with some figures
486 and Guo-Chen Leu provided some CWB results. Chung-Chieh Wang prepared the manuscript with contributions from
487 all co-authors.

Competing interests

489 The authors declare that they have no conflict of interest.

Acknowledgments

Constructive comments and suggestions from two anonymous reviewers and Prof. George Tai-Jen Chen of the National Taiwan University are appreciated. The first author, CCW, wishes to thanks assistants Ms. Y.-W. Wang, Mr. T.-C. Lin, and Mr. K.-Y. Chen for their help on this study. The CWB is acknowledged for providing the observational data, the radar plots, and the QPF verification results in Fig. 2. The National Center for High-performance Computing (NCHC) and the Taiwan Typhoon and Flood Research Institute (TTFRI) provided the computational resources. This study is jointly supported by the Ministry of Science and Technology of Taiwan under Grants MOST-103-2625-M-003-001-MY2, MOST-105-2111-M-003-003-MY3, MOST-108-2111-M-003-005-MY2, MOST-110-2111-M-003-004, and MOST-110-2625-M-003-001.

References

Barnes, L. R., Schultz, D. M., Gruntfest, E. C., Hayden, M. H., and Benight, C. C.: Corrigendum: False alarm rate or false alarm ratio?, Weather Forecast., 24, 1452–1454, https://doi.org/10.1175/2009WAF2222300.1, 2009.

Bryan, G. H., Wyngaard, J. C., and Fritsch, J. M.: Resolution requirements for the simulation of deep moist convection, Mon. Weather Rev., 131, 2394–2416, https://doi.org/10.1175/1520-0493(2003)131%3C2394:RRFTSO%3E2.0.CO;2, 2003.

Chang, C.-P., Yeh, T.-C., and Chen, J.-M.: Effects of terrain on the surface structure of typhoons over Taiwan, Mon. Weather Rev., 121, 734–752, https://doi.org/10.1175/1520-0493(1993)121%3C0734:EOTOTS%3E2.0.CO;2, 1993.

Chang, C.-P., Yang, Y.-T., and Kuo, H.-C.: Large increasing trend of tropical cyclone rainfall in Taiwan and the roles of terrain, J. Clim., 26, 4138–4147, https://doi.org/10.1175/JCLI-D-12-00463.1, 2013.

Chen, C.-S., and Chen, Y.-L.: The rainfall characteristics of Taiwan. Mon. Weather Rev., 131, 1324–1341, 2003.

Chen, G. T.-J., Wang, C-C., and Lin, D. T.-W.: Characteristics of low-level jets over northern Taiwan in Mei-yu season and their relationship to heavy rain events, Mon. Weather Rev., 133, 20–43, https://doi.org/10.1175/MWR-2813.1, 2005.

Chen, T.-C., Yen, M.-C., Hsieh, J.-C., and Arritt, R. W.: Diurnal and seasonal variations of the rainfall measured by the Automatic Rainfall and Meteorological Telemetry System in Taiwan. Bull. Amer. Meteor. Soc., 80, 2299–2312, doi:10.1175/1520-0477(1999)080,2299: DASVOT.2.0.CO;2, 1999.

Cheung, K. K. W., Huang, L.-R., and Lee, C.-S.: Characteristics of rainfall during tropical cyclone periods in Taiwan, Nat. Hazards Earth Syst. Sci., 8, 1463–1474, https://doi.org/10.5194/nhess-8-1463-2008, 2008.

Chi, S.-S.: The Mei-Yu in Taiwan, SFRDEST E-06-MT-03-4, Chung-Shin Engineering Technology Research and Development Foundation, Taipei, Taiwan, 65 pp, 2006. (in Chinese)

Chien, F.-C., and Jou, B. J.-D.: MM5 ensemble mean precipitation in the Taiwan area for three early summer convective (Mei-Yu) seasons, Weather Forecast., 19, 735–750, 2004.

Chien, F.-C., Kuo, Y.-H., and Yang, M.-J.: Precipitation forecast of MM5 in the Taiwan area during the 1998 Mei-yu season, Weather Forecast., 17, 739–754, https://doi.org/10.1175/1520-0434(2002)017%3C0739:PFOMIT%3E2.0.CO;2, 2002.

525 Chien, F.-C., Liu, Y.-C., and Jou, B. J.-D.: MM5 ensemble mean forecasts in the Taiwan area for the 2003 Mei-yu
526 season, Weather Forecast., 21, 1006–1023, https://doi.org/10.1175/WAF960.1, 2006.

527 Clark, A. J., Gallus, Jr., W. A., and Chen, T.-C.: Comparison of the diurnal precipitation cycle in convection-resolving
528 and non-convection-resolving mesoscale models, Mon. Weather Rev., 135, 3456–3473,
529 https://doi.org/10.1175/MWR3467.1, 2007.

530 Clark, A. J., Kain, J. S., Stensrud, D. J., Xue, M., Kong, F., Coniglio, M. C., Thomas, K. W., Wang, Y., Brewster, K.,
531 Gao, J., Wang, X., Weiss, S. J., and Du, J.: Probabilistic precipitation forecast skill as a function of ensemble size and
532 spatial scale in a convection-allowing ensemble, Mon. Weather Rev., 139, 1410–1418,
533 https://doi.org/10.1175/2010MWR3624.1, 2011.

534 Cotton, W. R., Tripoli, G. J., Rauber, R. M., and Mulvihill, E. A.: Numerical simulation of the effects of varying ice
535 crystal nucleation rates and aggregation processes on orographic snowfall, J. Appl. Meteorol. Climatol., 25, 1658–
536 1680, https://doi.org/10.1175/1520-0450(1986)025%3C1658:NSOTEO%3E2.0.CO;2, 1986.

537 Cuo, L., Pagano, T. C., and Wang, Q. J.: A review of quantitative precipitation forecasts and their use in short- to
538 medium-range streamflow forecasting, J. Hydormeteorol., 12, 713–728, https://doi.org/10.1175/2011JHM1347.1,
539 2011.

540 Davis, C., Brown, B., and Bullock, R.: Object-based verification of precipitation forecasts. Part I: Methodology and
541 application to mesoscale rain areas, Mon. Weather Rev., 134, 1772–1784, https://doi.org/10.1175/MWR3145.1, 2006.

542 Deardorff, J. W.,: Stratocumulus-capped mixed layers derived from a three-dimensional model, Bound.-Layer
543 Meteorol., 18, 495–527, 1980.

544 Done, J., Davis, C. A., and Weisman, M.: The next generation of NWP: explicit forecasts of convection using the
545 weather research and forecasting (WRF) model, *Atmos. Sci. Lett.*, *5*, 110–117, 2004.

546 Ebert, E. E.: Ability of a poor man's ensemble to predict the probability and distribution of precipitation, Mon.
547 Weather Rev., 129, 2461–2480, https://doi.org/10.1175/1520-0493(2001)129%3C2461:AOAPMS%3E2.0.CO;2,
548 2001.

549 Ebert, E. E., and McBride, J. L.: Verification of precipitation in weather systems: Determination of systematic errors,
550 J. Hydrol., 239, 179–202, https://doi.org/10.1016/S0022-1694(00)00343-7, 2000.

551 Ebert, E. E., Damrath, U., Wergen, W., and Baldwin, M. E.: The WGNE assessment of short-term quantitative
552 precipitation forecasts (QPFs) from operational numerical weather prediction models, Bull. Am. Meteorol. Soc., 84,
553 481–492, https://doi.org/10.1175/BAMS-84-4-481, 2003.

554 Fang, X., and Kuo, Y.-H.: Improving ensemble-based quantitative precipitation forecasts for topography-enhanced
555 typhoon heavy rainfall over Taiwan with a modified probability-matching technique, Mon. Weather Rev., 141, 3908–
556 3932, https://doi.org/10.1175/MWR-D-13-00012.1, 2013.

557 Fritsch, J. M., and Carbone, R. E.: Improving quantitative precipitation forecasts in the warm season. A USWRP
558 research and development strategy, Bull. Am. Meteorol. Soc., 85, 955–965, https://doi.org/10.1175/BAMS-85-7-955,
559 2004.

560 Gilleland, E., Ahijevych, D. A., Brown, B. G., and Ebert, E. E.: Verifying forecasts spatially, Bull. Am. Meteorol.
561 Soc., 91, 1365–1373, https://doi.org/10.1175/2010BAMS2819.1, 2010.

562   Golding, B. W.: Quantitative precipitation forecasting in the UK. J. Hydrol., 239, 286–305,
563   https://doi.org/10.1016/S0022-1694(00)00354-1, 2000.

564   Hochman, A., Scher, S., Quinting, J., Pinto, J. G., and Messori, G.: A new view of heat wave dynamics and
565   predictability over the eastern Mediterranean, Earth Syst. Dynam., 12, 133–149, https://doi.org/10.5194/esd-12-133-
566   2021, 2021.

567   Hong, J.-S.: Evaluation of the high-resolution model forecasts over the Taiwan area during GIMEX, Weather and
568   Forecast., 18, 836–846, https://doi.org/10.1175/1520-0434(2003)018%3C0836:EOTHMF%3E2.0.CO;2, 2003.

569   Hong, J.-S., Fong, C.-T., Hsiao, L.-F., Yu, Y.-C., and Tseng, C.-Y.: Ensemble typhoon quantitative precipitation
570   forecasts model in Taiwan, Weather Forecast., 30, 217–237, https://doi.org/10.1175/WAF-D-14-00037.1, 2015.

571   Hsu, J.: ARMTS up and running in Taiwan, Väisälä News, 146, 24–26, 1998.

572   Hsu, J. C.-S., Wang, C.-J., Chen, P.-Y., Chang, T.-H., and Fong, C.-T. (2014), Verification of quantitative
573   precipitation forecasts by the CWB WRF and ECMWF on 0.125° grid, in: Proceedings of 2014 Conference on
574   Weather Analysis and Forecasting, Central Weather Bureau, Taipei, Taiwan, 16-18 September 2014, A2-24, 2014.
575   (in Chinese)

576   Huang, T.-S., Yeh, S.-H., Leu, G.-C., and Hong, J.-S.:, A synthesis and comparison of QPF verifications at the CWB
577   and major NWP guidance, in: Proceedings of 2015 Conference on Weather Analysis and Forecasting, Central Weather
578   Bureau, Taipei, Taiwan, 15-17 September 2015, A7-11, 2015. (in Chinese)

579   Huang, T.-S., Yeh, S.-H., Leu, G.-C., and Hong, J.-S.: Postprocessing of ensemble rainfall forecasts---Ensemble mean,
580   probability matched mean and exceeding probability, Atmospheric Sciences, 44, 173–196, 2016. (in Chinese with
581   English abstract)

582   Ikawa, M., and Saito, K: Description of a non-hydrostatic model developed at the Forecast Research Department of
583   the MRI, Technical Report, 28, Meteorological Research Institute, Tsukuba, Ibaraki, Japan, 245 pp, 1991.

584   Jou, B. J.-D., Lee, W.-C., and Johnson, R. H.: An overview of SoWMEX/TiMREX, in: The Global Monsoon System:
585   Research and Forecast, 2nd Edition, edited by: Chang, C.-P., Ding, Y., Lau, N.-C., Johnson, R. H., Wang, B., Yasunari,
586   T., World Scientific, Toh Tuck Link, Singapore, 303–318, https://doi.org/10.1142/9789814343411_0018, 2011.

587   Kalnay, E., Kanamitsu, M., and Baker, W. E.: Global numerical weather prediction at the National Meteorological
588   Center, Bull. Am. Meteorol. Soc., 71, 1410–1428, 1990.

589   Kanamitsu, M.: Description of the NMC global data assimilation and forecast system, Weather Forecast., 4, 335–342,
590   https://doi.org/10.1175/1520-0434(1989)004%3C0335:DOTNGD%3E2.0.CO;2, 1989.

591   Kleist, D. T., Parrish, D. F., Derber, J. C., Treadon, R., Wu, W. S., and Lord, S.: Introduction of the GSI into the
592   NCEP   global   data   assimilation   system,   Weather   Forecast.,   24,   1691–1705,
593   https://doi.org/10.1175/2009WAF2222201.1, 2009.

594   Kondo, J.: Heat balance of the China Sea during the air mass transformation experiment, J. Meteor. Soc. Japan, 54,
595   382–398, https://doi.org/10.2151/jmsj1965.54.6_382, 1976.

596   Kuo, Y.-H., and Chen, G. T.-J.: The Taiwan Area Mesoscale Experiment (TAMEX): An overview, Bull. Am.
597   Meteorol. Soc., 71, 488–503, http://dx.doi.org/10.1175/1520-0477(1990)071%3C0488:TTAMEA%3E2.0.CO;2,
598   1990.

599   Li, C.-H., and Hong, J.-S.: Study on the application and analysis of regional ensemble quantitative precipitation

600   forecasts, in: Proceedings of 2014 Conference on Weather Analysis and Forecasting, Central Weather Bureau, Taipei,

601   Taiwan, 16-18 September 2014, A2-19, 2014. (in Chinese)

602   Li, J. and Chen, Y.-L.: Barrier jets during TAMEX, Mon. Weather Rev., 126, 959–971, https://doi.org/10.1175/1520-

603   0493(1998)126%3C0959:BJDT%3E2.0.CO;2, 1998.

604   Lin, Y.-L., Farley, R. D., and Orville, H. D.: Bulk parameterization of the snow field in a cloud model, J. Appl.

605   Meteorol. Climatol., 22, 1065–1092, https://doi.org/10.1175/1520-0450(1983)022%3C1065:BPOTSF%3E2.0.CO;2,

606   1983.

607   Louis, J. F., Tiedtke, M., and Geleyn, J. F.: A short history of the operational PBL parameterization at ECMWF, in:

608   Proceedings of Workshop on Planetary Boundary Layer Parameterization, Shinfield Park, Reading, UK, 25-27

609   November 1981, 59–79, 1982.

610   Moorthi, S., Pan, H. L., and Caplan, P.: Changes to the 2001 NCEP operational MRF/AVN global analysis/forecast

611   system, NWS Technical Procedures Bulletin, 484, Office of Meteorology, National Weather Service, Silver Spring,

612   Maryland, USA, 2001.

613   Murakami, M.: Numerical modeling of dynamical and microphysical evolution of an isolated convective cloud---The

614   19 July 1981 CCOPE cloud, J. Meteor. Soc. Japan, 68, 107–128, https://doi.org/10.2151/jmsj1965.68.2_107, 1990.

615   Murakami, M., Clark, T. L., and Hall, W. D.: Numerical simulations of convective snow clouds over the Sea of Japan:

616   Two-dimensional simulation of mixed layer development and convective snow cloud formation, J. Meteor. Soc. Japan,

617   72, 43–62, https://doi.org/10.2151/jmsj1965.72.1_43, 1994.

618   Paul, S., Wang, C.-C., Chien, F.-C., and Lee, D.-I.: An evaluation of the WRF Mei-yu rainfall forecasts in Taiwan,

619   2008-2010: differences in elevation and sub-regions. Meteorol. Appl., 25, 269-282, doi: 10.1002/met.1689, 2018.

620   Roberts, N. M., and Lean, H. W.: Scale-selective verification of rainfall accumulations from high-resolution forecasts

621   of convective events, Mon. Weather Rev., 136, 78–97, https://doi.org/10.1175/2007MWR2123.1, 2007.

622   Roebber, P. J.: Visualizing multiple measures of forecast quality, Weather Forecast., 24, 601–608,

623   https://doi.org/10.1175/2008WAF2222159.1, 2009.

624   Schaefer, J. T.: The critical success index as an indicator of warning skill, Weather Forecast., 5, 570–575,

625   https://doi.org/10.1175/1520-0434(1990)005%3C0570:TCSIAA%3E2.0.CO;2, 1990.

626   Segami, A., Kurihara, K., Nakamura, H., Ueno, M., Takano, I., and Tatsumi, Y.: Operational mesoscale weather

627   prediction with Japan Spectral Model, J. Meteor. Soc. Japan, 67, 907–924, https://doi.org/10.2151/jmsj1965.67.5_907,

628   1989.

629   Skamarock, W. C., Klemp, J. B., Dudhia, J., Gill, D. O., Barker, D. M., Wang, W., and Powers, J. G.: A description

630   of the advanced research WRF version 2, National Center for Atmospheric Reasearch, Boulder, Colorado, USA, 88

631   pp, http://dx.doi.org/10.5065/D6DZ069T, 2005.

632   Su, Y.-J., Hong, J.-S., and Li, C.-H.: The characteristics of the probability matched mean QPF for 2014 Meiyu season,

633   Atmospheric Sciences, 44, 113-134, 2016. (in Chinese with English abstract)

634 Tsuboki, K., and Sakakibara, A.: Large-scale parallel computing of cloud resolving storm simulator, in: High
635 Performance Computing, edited by: Zima H. P., Joe K., Sato M., Seo Y., Shimasaki M., Springer, Berlin, Heidelberg,
636 Germany, 243–259, https://doi.org/10.1007/3-540-47847-7_21, 2002.

637 Tsuboki, K., and Sakakibara, A.: Numerical Prediction of High-Impact Weather Systems: The Textbook for the
638 Seventeenth IHP Training Course in 2007, Hydrospheric Atmospheric Research Center, Nagoya University, Nagoya,
639 Japan, and UNESCO, Paris, France, 273 pp, 2007.

640 Walser, A., and Schär, C.: Convection-resolving precipitation forecasting and its predictability in Alpine river
641 catchments, J. Hydrol., 288, 57–73, https://doi.org/10.1016/j.jhydrol.2003.11.035, 2004.

642 Wang, C.-C.: On the calculation and correction of equitable threat score for model quantitative precipitation forecasts
643 for small verification areas: The example of Taiwan, Weather Forecast., 29, 788–798, https://doi.org/10.1175/WAF-
644 D-13-00087.1, 2014.

645 Wang, C.-C.: The more rain, the better the model performs—The dependency of quantitative precipitation forecast
646 skill on rainfall amount for typhoons in Taiwan, Mon. Weather Rev., 143, 1723–1748, https://doi.org/10.1175/MWR-
647 D-14-00137.1, 2015.

648 Wang, C.-C.: News and notes, Paper of notes: The more rain from typhoons, the better the models perform, Bull. Am.
649 Meteorol. Soc., 97, 16–17, https://doi.org/10.1175/BAMS_971_11-18_Nowcast, 2016.

650 Wang, C.-C., Chen, G. T.-J., Chen, T.-C., and Tsuboki, K.: A numerical study on the effects of Taiwan topography
651 on a convective line during the mei-yu season, Mon. Weather Rev., 133, 3217–3242,
652 https://doi.org/10.1175/MWR3028.1, 2005.

653 Wang, C.-C., Chen, G. T.-J., and Huang, S.-Y.: Remote trigger of deep convection by cold outflow over the Taiwan
654 Strait in the Mei-yu season: A modeling study of the 8 June 2007 Case, Mon. Weather Rev., 139, 2854–2875,
655 https://doi.org/10.1175/2011MWR3613.1, 2011.

656 Wang, C.-C., Kung, C.-Y., Lee, C.-S., and Chen, G. T.-J.: Development and evaluation of Mei-yu season quantitative
657 precipitation forecast in Taiwan river basins based on a conceptual climatology model, Weather Forecast., 27, 586–
658 607, https://doi.org/10.1175/WAF-D-11-00098.1, 2012a.

659 Wang, C.-C., Kuo, H.-C., Chen, Y.-H., Huang, H.-L., Chung, C.-H., and Tsuboki, K.: Effects of asymmetric latent
660 heating on typhoon movement crossing Taiwan: The case of Morakot (2009) with extreme rainfall, J. Atmos. Sci., 69,
661 3172–3196, https://doi.org/10.1175/JAS-D-11-0346.1, 2012b.

662 Wang, C.-C., Chen, Y.-H., Kuo, H.-C., and Huang, S.-Y.: Sensitivity of typhoon track to asymmetric latent
663 heating/rainfall induced by Taiwan topography: A numerical study of Typhoon Fanapi (2010), J. Geophys. Res.
664 Atmos., 118, 3292–3308, https://doi.org/10.1002/jgrd.50351, 2013a.

665 Wang, C.-C., Kuo, H.-C., Yeh, T.-C., Chung, C.-H., Chen, Y.-H., Huang, S.-Y., Wang, Y.-W., and Liu, C.-H.: High-
666 resolution quantitative precipitation forecasts and simulations by the Cloud-Resolving Storm Simulator (CReSS) for
667 Typhoon Morakot (2009), J. Hydrol., 506, 26–41. https://doi.org/10.1016/j.jhydrol.2013.02.018, 2013b.

668 Wang, C.-C., Huang, S.-Y., Chen, S.-H., Chang, C.-S., and Tsuboki, K.: Cloud-resolving typhoon rainfall ensemble
669 forecasts for Taiwan with large domain and extended range through time-lagged approach, Weather Forecast., 31,
670 151–172, https://doi.org/10.1175/WAF-D-15-0045.1, 2016a.

671   Wang, C.-C., Chiou, B.-K., Chen, G. T.-J., Kuo, H.-C., and Liu, C.-H.: A numerical study of back-building process

672   in a quasistationary rainband with extreme rainfall over northern Taiwan during 11-12 June 2012, Atmos. Chem. Phys.,

673   16, 12359–12382, https://doi.org/10.5194/acp-16-12359-2016, 2016b.

674   Wang, C.-C., Paul, S., Chien, F.-C., Lee, D.-I., and Chuang, P.-Y.: An evaluation of WRF rainfall forecasts in Taiwan

675   during three mei-yu seasons of 2008-2010, Weather Forecast., 32, 1329–1351, https://doi.org/10.1175/WAF-D-16-

676   0190.1, 2017.

677   Wernli, H., Paulat, M., Hagen, M., and Frei, C.: SAL－A novel quality measure for the verification of quantitative

678   precipitation forecasts, Mon. Weather Rev., 136, 4470–4487, https://doi.org/10.1175/2008MWR2415.1, 2008.

679   Wilks, D. S.: Statistical methods in the atmospheric sciences, 3rd Edition. Academic Press, San Diego, California,

680   USA, 2011.

681   Wu, C.-C., and Kuo, Y.-H.: Typhoons affecting Taiwan: Current understanding and future challenges, Bull. Am.

682   Meteorol. Soc., 80, 67–80, https://doi.org/10.1175/1520-0477(1999)080%3C0067:TATCUA%3E2.0.CO;2, 1999.

683   Yang, M.-J., Jou, B. J.-D., Wang, S.-C., Hong, J.-S., Lin, P.-L., Teng, J.-H., and Lin, H.-C.: Ensemble prediction of

684   rainfall during the 2000–2002 mei-yu seasons: Evaluation over the Taiwan area, J. Geophys. Res., 109, D18203,

685   https://doi.org/10.1029/2003JD004368, 2004.

686   Yeh, H.-C., and Chen, Y.-L.: Characteristics of the rainfall distribution over Taiwan during TAMEX, J. Appl.

687   Meteorol. Climatol., 37, 1457–1469, https://doi.org/10.1175/1520-0450(1998)037%3C1457:CORDOT%3E2.0.CO;2,

688   1998.

689   Yeh, H.-C., and Chen, Y.-L.: The role of off shore convergence on coastal rainfall during TAMEX IOP 3, Mon.

690   Weather Rev., 130, 2709–2730, https://doi.org/10.1175/1520-0493(2002)130%3C2709:TROOCO%3E2.0.CO;2,

691   2002.